NBSIR 79-1910

Purely Buoyant Diffusion Flames: Some Experimental Results

Bernard J. McCaffrey

Center for Fire Research
National Engineering Laboratory
National Bureau of Standards
Washington, D.C. 20234

October 1979

Final Report

U.S. DEPARTMENT OF COMMERCE

NATIONAL BUREAU OF STANDARDS

NBSIR 79-1910

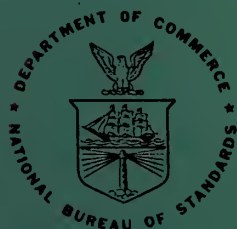# PURELY BUOYANT DIFFUSION FLAMES: SOME EXPERIMENTAL RESULTS

Bernard J. McCaffrey

Center for Fire Research
National Engineering Laboratory
National Bureau of Standards
Washington, D.C. 20234

October 1979

Final Report

TABLE OF CONTENTS

LIST OF TABLES

LIST OF FIGURES

b   intercept (at burner) of $x_{1/e}$ vs z width line, m

c_p specific heat, J/kg K

C   buoyancy constant $= V/\sqrt{2gz\Delta T/T_o}$

d_o diameter of burner, m

F_o source Froude number $- u_o^2/g\, d_o$

F_o source buoyancy rate parameter $- gQ/(\rho_o c_p T_o)$

g   gravitational acceleration, 9.8 m/s^2

h   convective film coefficient, kW/m^2 K

k   coefficients for center line correlations, various dimensions

η exponent of center line correlations

m   slope of $x_{1/e}$ vs z width line

n   exponent of exponential radial profiles

Δp total or stagnation pressure minus static pressure, N/m^2

Q   nominal heat release rate or net calorific potential of fuel gas, kW

r_o radius of burner, m

T   absolute temperature, °K

ΔT temperature rise above ambient, °C

u_o velocity of gas leaving burner surface, m/s

V,v   flow velocity, m/s

x   traverse distance from center line, m

$x_{1/e}$ distance from center line where the value of the variable equals 1/e of the value on the center line, m

z   vertical height above burner, m

ε_g effective gaseous emissivity

ρ density, kg/m^3

τ averaging time, s

τ_a auto-correlation time delay, s

Subscripts

o   ambient

o   center line values

o   initial conditions at burner surface

v   designating velocity profile when referenced to $x_{1/e}$

ΔT designating temperature profile when referenced to $x_{1/e}$

c   designating buoyancy profile when referenced to $x_{1/e}$

Superscripts

-     time-averaged values

'   instantaneous values

PURELY BUOYANT DIFFUSION FLAMES: SOME EXPERIMENTAL RESULTS

Bernard J. McCaffrey

Abstract

Measurements of temperature and velocity using
thermocouples and an impact probe were made in the near
field of a purely buoyant diffusion flame produced by
a porous refractory burner. Based on time-averaged
center line value of V and ΔT together with photographic
records the flame can be conveniently divided into three
distinct regimes: (1) a continous flame region, starting
from the surface of the burner with V equal to zero at
the surface and rising with the height above the burner,
z, to the 1/2 power. ΔT is constant over this regime.
Higher up is (2), an intermittent regime, with pulsating
flame (~ 3 Hz) exhibiting approximately constant V and
ΔT falling with z to the first power. Still higher is
(3) the plume region which is, most of the time, free of
flames with $V \sim z^{-1/3}$ and $\Delta T \sim z^{-5/3}$ as predicted by
conventional plume theory. Throughout the three regimes
and indistinguishable among these is the consistency of
the buoyancy relation, $V/\sqrt{2gz\Delta T/T_o}$ which has a value
of approximately 0.9, a factor of 2.5 times previous
estimates in the flame region and confirming the recent
correlation measurements of Cox [1][1]. Different heat
release rates, Q, can be scaled to a "universal" fire if
the length is normalized as $z/Q^{2/5}$ and the velocity scale
as $V/Q^{1/5}$. The flame regime is thus independent of Q.

In the radial direction for time-averaged quantities
only the plume region appears reasonably Gaussian. The
data in the flame and intermittent regimes do not fall
as rapidly as that dictated by a Gaussian distribution.
In all three regimes the velocity profile is _wider_ than
the temperature profile.

Large scale, low frequency Δp fluctuations are
about 35% of the time-averaged signal on the center line
throughout the three regions. Radially the fluctuating

---

[1]Numbers in brackets refer to literature references listed at the end of
this report.

to time-averaged signal ratio rises from the center line value and approaches 100% in the wings. Elementary spectral analysis indicates that most of this energy is concentrated in a narrow band centered around 3 Hz.

Implications of these results for flame entrainment calculations and heat release rates will be discussed.

Key words: Buoyancy; diffusion flames; fire entrainment; flame oscillations; plume; scaling.

1. INTRODUCTION

Most studies of diffusion flames have been concerned with combustion systems having fuel source injection rates characterized by high initial momentum; the gas leaves the burner surface with substantial velocity in a jet-like manner. A free burning fire' such as would occur over a liquid pool or slab of polymeric material, on the other hand, will be totally dominated by buoyancy; the fuel leaves the surface with negligible velocity. To date no satisfactory analytical scheme appears capable of accommodating buoyancy with combustion and few experimental results exist for these diffusion flames especially in the near field (the region immediately adjacent to the fuel source). Point source plume theory which is expected to be valid far from the source will be inadequate in this region for most finite-size fires, e.g., in an enclosure fire situation the flames will extend to a significant portion of the height of the enclosure. The region of interest in this case is the accelerating near field. Radiation, the size of combustion zones and flame length, air entrainment, mixing and other physiochemical processes governing the behavior of these fires are not well understood. Accurate knowledge of the flow in the accelerating region may lead to better understanding of these phenomena.

Spatial and temporal non-uniformity due to large-scale, low frequency eddy motion with little preferred direction, especially at the edges of the flame, coupled with the tendency of these systems to be very susceptible to ambient disturbances makes measurements and their interpretation extremely difficult. Cox, at the Fire Research Station, Borehamwood, England where most of the present measurements were made, is using cross correlation techniques to probe the flame. Terai [2] also using cross correlation is investigating the near field of finite-size pool fires. Heskestad [3] has made some measurements using a pitot-static tube approaching the flame

2

region of both a wood crib and a methanol pan fire. Yokoi [4] in a classic
study of the subject has made temperature measurements in the flame above a
finite area source.

The purpose of the present work is to add to and extend the utility of
the above collection of data. Modeling schemes will remain suspect until a
reliable set of data becomes available which will provide comparisons at
least for the gross structure of buoyant diffusion flames. There are in
addition short term requirements of fire research which necessitate the
quantitative understanding of air entrainment in order to complete the flow
portion of Enclosure Fire Models [5].

The present study consists of measurements made in the flame of a
single burner where the amount of gas could be varied thus simulating
materials with different burning rates per unit area. Source Froude number
($F_o = u_o^2/g\,d_o$) varied from about 10^{-6} to 10^{-4} thus insuring a simulation
of truly buoyant behavior.

2. INSTRUMENTATION AND PROCEDURE

The burner using natural gas (35 kJ/ℓ) at various controlled rates was
constructed of a porous refractory material 0.30 m square. It sat 0.75 m
above the floor and under a passive hood in a large laboratory. Visually
non-axisymmetric behavior could be observed only very close to the burner
surface. The instrumentation was located over the center line of the burner
using a plumb bob. Thereafter, vertical and side to side movement of the
instrument cluster was accomplished with a micrometer lathe-type movement
device which held the pressure probe and thermocouple.

Velocity was measured using a bidirectional pressure probe [6] which
responds like a pitot-static probe except the measuring area is quite large
(0.016 m diameter) which spatially averages the signals in order to obtain
the gross structure of the flame. In addition to the spatial averaging,
the output of the electronic manometer was time-averaged through a filtering
voltmeter where averaging times of up to 100 s were possible. This was
quite sufficient for a steady center line reading. In the wings of the
flame however, additional averaging was required due to ambient disturbances
and this was accomplished by taking the 100 s averaged output and displaying
it on a slow writing oscillograph and observing the signals for several
minutes until a faired signal could be obtained. No attempt was made to
totally isolate the flame from laboratory disturbances. The extent and
duration of disturbances could be monitored both visually and from the
oscillograph, and data recorded during these distrubances was not used.

Temperature rise was measured using a large thermocouple (1.0 mm SS sheath) with the chromel-alumel junction welded to the sheath (nominal time constant approx. 3 s). No further damping was provided. The thermocouple (mv) reading was displayed similar to the time-averaged pressure signal on the slow writing oscillograph. Again, a faired averaged value of ΔT was then obtained. The majority of the results presented here are for time-averaged quantities; instantaneous values of pressure are discussed in the appropriate section of the text.

There are notable difficulties with this kind of measurement of velocity, i.e., using pressure and temperature for density. Firstly, in the high temperatures of the flame the Reynolds number of the flow around the pressure probe can go as low as a couple of hundred. Reference 6 contains a low Reynolds number calibration which could be used to correct for these effects. The results would be a maximum velocity error of about + 15% near the burner surface with the error decreasing in going further above the surface where velocities are rising. However, the calibration was not used due to the strong oscillatory nature of the pressure signal (see "Nature of the Signals" in Results Section). The thickening boundary layer associated with lower Reynolds numbers may not be sustained due to the strong pulsations at 3 Hz present in the flow field.

Secondly, pulsations and turbulence can cause significant errors in the measurement of velocity using pressure probes. For a nonlinear relationship between signal and measurement property ($\Delta p = KV^2$) an error will be generated in the time-mean property of a fluctuating flow. For constant density and when the pulsating frequency is low compared with the turbulence frequencies this error can be shown to be small, e.g., 4% for a 40% RMS amplitude of velocity oscillation. However, the flame situation is not so simple. At any position in a stationary flame the time-mean values of density and velocity are constant but both may fluctuate independently and in unknown correlation. Taking the time average of $(\bar{\Delta p} + \Delta p') = K(\bar{\rho} + \rho')(\bar{V} + V')^2$, for example, will lead to indeterminate correlations even ignoring composition changes. The scale and intensity of turbulence is virtually unknown in the lower regions of these systems.

The large size and slow time response of the instruments may tend to help diminish the effects of this fine scale energy until some of these effects may be resolved in future work.

Finally, thermocouple errors due to strong radiative interaction will be difficult to assess. The center line value of temperature indicated

4

by the thermocouple will tend to be lower than the actual flame or gas
temperature due to radiation from the thermocouple through the gas to the
surroundings. These errors will be minimized in areas where the gaseous
absorption coefficient is high (thickest flames) and the convective coef-
ficient is high (velocity high). Coming up out of the flame the local
absorption coefficient will probably be decreasing whereas the velocity
will be increasing and hence the two will tend to compensate. Also radiation
error will decrease significantly still further up where the temperature is
falling significantly. The order of error for these typical flame conditions
will be about 20% at T_{gas} = 1300 K assuming h ~ 0.1 kw/m^{2}K and ε_g ~ 0.15.
The thermocouple will be reading about 1000 K.

In the wings the radiation error will be in the opposite direction,
the indicated temperature will be higher than the true gas temperature.
The thermocouple will be out of physical contact with the flames in the
slower moving entrained and mixed gases and will be dominated by radiation
from the nearby "wall" of flames. Future measurements using different size
thermocouple beads as well as an aspirated probe will be required to
accurately assess errors and effective gaseous emissivities in the radial
direction. Fortunately, in the calculation of velocity the square root of
the absolute temperature is used and hence in the wings, as the temperature
approaches ambient, the thermocouple errors will not be critical.

In spite of all these difficulties the pressure probe should provide a
simple means of obtaining the gross structure of the flames in the form of
a consistent set of data which can be modified as more refined and detailed
information about buoyant combustion becomes available. Velocity will be
calculated as a constant times the square root of the product of the time-
averaged differential pressure and the time-averaged absolute temperature.

3. RESULTS AND DISCUSSION

3.1 Center Line Velocity and Temperature Rise

Figures 1 and 2 present the time-averaged center line velocity and
temperature against height above the burner, z, for five values of gas
flow, Q. (Hereafter Q will be referred to as the heat release rate or fire
size even though in fact it is only the calorific potential supplied to the
burner). The scaling factors $Q^{1/5}$ and $Q^{2/5}$ for V and z are purely empirical
findings - coming directly from a consideration of log-log plots of V and
ΔT against z for the individual fire sizes. Upon plotting V and ΔT versus
z (not shown), two regimes of data immediately become clear. For large

5

values of z, the plume region, the data exhibit the characteristic $z^{-1/3}$ and $z^{-5/3}$ variation for V and ΔT dependence. The other region is for the points in the flame, small z, which show a remarkable tendency to cluster around a line with slope plus 1/2 for V and zero for ΔT. Using cross correlation of temperature and flame ionization fluctuations Cox found the identical behavior. Drawing a line through only points that are obviously in the plume and another through only points which belong to the $\eta = 1/2$ or flame regime leads to an intersection falling higher than the intermediate points which belong to neither regime. This intersection will define a velocity, V_i which will be higher than the data and a height, z_i. There will be two z_i's: one from the velocity plot and one from the temperature plot (the constant flame temperature intersecting with the $z^{-5/3}$ plume line will define another z_i but not a ΔT_i since that is the flame temperature extended). The two z_i's turn out to be nearly identical. If this is done for all the different Q's, and then V_i and z_i for each are plotted against Q the result will be that V_i will vary with Q to the 1/5 power and z_i with Q to the 2/5 power, thus establishing the proper scaling. If instead of a single z_i two values of z for each Q are chosen corresponding to the location where the data ceases to follow firstly, the flame $z^{1/2}$ line, and secondly, the plume $z^{-1/3}$ line, then these can be plotted against Q. Both of these again result in a $Q^{2/5}$ relation. Like z_i there will be an additional set of intersections from the temperature data. The agreement between the velocity and temperature derived values of z_i at the intersections is good.

The functional relationship of V and ΔT with z in the intermittent regime is not as straightforward as it is in the other two regions. For convenience a zero slope for V and a slope of -1 for ΔT was arbitrarily chosen. In reality these may vary, i.e., the actual velocity relationship is probably a curving line or cap connecting the flame and plume rather than the straight line with two sharp transitions. What is clear however is that the buoyancy relation $V/\sqrt{2gz\Delta T/T_o}$ = constant must guide any choice in this regime as well as the other two[2]. Substituting the data, i.e., values of V and ΔT, into this expression will result in a constant at all values of z. The constant is preserved point by point throughout the entire field and hence V(z) and $\Delta T(z)$ must be consistent.

The points on figures 1 and 2 which fall below the $z^{1/2}$ line of V and the constant ΔT vs z line were for z very close to the burner surface

---

[2]For a simple hydrostatic pressure variation $p = p_o - g \int_o^z \rho \, dz$ or $\Delta p \sim -g\Delta\rho z$.

Using Bernoulli's equation and the ideal gas relation, this becomes:

$1/2 \, \rho V^2 \sim g\rho_o \frac{\Delta T}{T} z$ or $V/\sqrt{2gz\Delta T/T_o} = C$.

(0.045 m) where a very fuel-rich condition exists in the center. It is
actually possible to see a cone-shaped region or core of non-luminous gas
just above the burner surface surrounded by a flame envelope near the
edges. The larger the gas flow the greater the deviation from the behavior
of the flame region further up, i.e., the greater the fuel-rich volume
above the burner.

Reiterating and relating the results to what one observes visually,
the purely buoyant diffusion flame above a finite area source can be
divided into three distinct regimes. In terms of time-averaged center line
velocity and temperature the lowest regime of continuous flame is character-
ized by constant temperature and a velocity starting off with a value of
zero at the burner surface and rising proportional to the height above the
burner to the 1/2 power. Above this zone the flame is intermittent in
appearance and clumps of visible flame are seen to rise periodically from
the continuous flame zone at a regular frequency of a few Hz. Velocity in
this region is nearly constant and temperature drops with height at a rate
proportional to the first power of z. At about the point where the "broken
off pieces" of flame of the intermittent region cease to be visible the
third region begins. Conventional plume theory ($V \sim z^{-1/3}$, $\Delta T \sim z^{-5/3}$)
describes this non-luminous region adequately.

Time-averaged center line velocity in all three regimes can therefore
be derived from static pressure differences due solely to buoyancy, i.e.,
$\sqrt{2gz\Delta T/T_o}$. The value of the proportionality constant is very high,
$V/\sqrt{2gz\Delta T/T_o} \sim 0.9$ and virtually invariant throughout, from the plume
region through the intermittent zone right down through continuous flames
to the base of the burner.

For larger and smaller fires from the same size source scaling with
the heat release rate, Q, will reduce all data to a universal curve. The
length scale becomes $z/Q^{2/5}$ and velocity is normalized as $V/Q^{1/5}$ with ΔT
invariant with Q when viewed in the proper length coordinate. The three
regimes then will be distinguished by two intersections or constant values
of $z/Q^{2/5}$. For the flame region alone both V and ΔT are independent of
fire size, Q, and presumably only dependent on burner area and fuel type.
Fire size enters only in determining how high or long this continuous flame
region will be.

Table 1 presents a summary of all the center line data and the weighted
average values of the coefficients of the various expressions found for the
three regimes from the five fire sizes. The solid lines on figures 1 and 2

are taken from table 1. Use of a third significant figure in the numbers
is probably optimistic here but perhaps might be useful in picking out
slight trends in such a large array of data.

In the flame region, which is independent of Q, the precision is
excellent, on the order of 1%. Note that those points in the fuel-rich
region very near the surface of the burner which fall below the major trend
of the data have been ignored. In the intermittent and plume regime there
exists a tendency for both temperature correlations, $\Delta T z/Q^{2/5}$ and $\Delta T z^{5/3}/Q^{2/3}$
to increase slightly with fire size resulting in a decrease in the buoyancy
relation, $V/\sqrt{2gz\Delta T/T_o}$. This tendency can be seen on figure 2 where the
higher Q points rise above the solid line. A possible reason for this
anomaly could be thermocouple (TC) radiation error decreasing with fire
size. Recall that center line temperature will read low. The width or base
of flames "seen" by the thermocouple from above will increase with Q. The
effect of this component will be more pronounced in the intermittent and
plume regimes. Note that velocity, as expected, appears to be little
affected by temperature error since V varies with the square root of the
absolute temperature whereas the buoyancy relation varies with the square
root of the temperature difference. The averages will be heavily weighted
toward the smallest fire (Q = 14.4 kW) since more data is available for it.
The errors in the final averages for temperature will therefore be in that
direction. A summary of the center line data is:

$$V/Q^{1/5} = k\left(\frac{z}{Q^{2/5}}\right)^{\eta} \qquad \frac{2g\Delta T}{T_o} = \left(\frac{k}{C}\right)^2 \left(\frac{z}{Q^{2/5}}\right)^{2\eta-1}$$

	k		η	$z/Q^{2/5}$ m/kW$^{2/5}$	
Flame	6.8	$\dfrac{m^{1/2}}{s}$	1/2	<0.08	
Intermittent	1.9	$\dfrac{m}{s\ kW^{1/5}}$	0	0.08-0.2	C = 0.9
Plume	1.1	$\dfrac{m^{4/3}}{s\ kW^{1/3}}$	-1/3	>0.2	

Both the flame-intermittent intersection $z/Q^{2/5}$ = 0.08 m kW$^{-2/5}$ and
the intermittent-plume intersection $z/Q^{2/5}$ = 0.20 m kW$^{-2/5}$ show good agree-
ment as calculated by velocity and temperature correlations. How well this
demarkation of regimes relates to what one might observe visually can be
seen in figure 3 where z is plotted against Q for the two intersections.
The lines are superimposed on 1 s time exposed photographs of the five
flames. One second exposure appears to be a good compromise between the
exposure being too fast and getting too few representative cycles of the
pulsating motion, and too slow and emphasizing atypical bursts of flame

outside a representative or average envelope. The 45 kW fire for example shows a large protrusion of flame beyond the marking stick on the right hand side of the picture, which is rarely present.

The tip of visible flame in the 1 s exposure comes just about equal or slightly lower than the velocity measurement-determined intermittent-plume intersection, $z/Q^{2/5} = 0.2$ m kW$^{-2/5}$, and hence this definition or criterion might lead to a less subjective or more quantitative measurement of flame length. Substituting this intersection into the correlation for temperature rise in either the intermittent or the plume region leads to a flame tip temperature rise of $\Delta T = 320°$ C which compares very favorably with previous work [7]. In that same study with a larger fire (250 kW) using a similar burner Thomas presents a flame height of 190 cm using mean values of the location of the flame tip from photographs. The present correlation would yield 0.2 x $(252)^{2/5} = 1.83$ m which is again slightly lower but probably within the scatter of the photographic records. Extrapolation of these flame length relationships to larger fires then would seem reasonable to at least a factor of five on heat release rate or source Froude number basis.

Nothing distinguishable, like flame height, can be observed on figure 3 for the lower, flame-intermittent intersection, $z/Q^{2/5} = 0.08$ m kW$^{-2/5}$, since the intermittent region will be completely exposed in a one-second photograph even for these low frequency pulsations. Consider, rather, figure 4 which shows a series of about one and one-third seconds of consecutive frames of motion-picture (24 frames/s) film of the flame. The heat release rate for this fire is 33 kW and the two intersections will be at 0.3 and 0.8 m. These can be located by the black flags on the measuring stick seen on the right side of the picture. The flags are 0.2 m apart. Most of the motion then should range midway between the first and second flag up to the fourth flag. Given the small sample size and the fact that the flame is seen in two dimensions, the contention that continuous flame exists up to 0.3 m is somewhat demonstrated in the photos. The nature of the intermittent regime is clearly illustrated. Note that the photos have been deliberately arranged in groups of eight each. (But they are consecutive, the first frame on the left in any row follows in time the last frame on the right in the previous row.) Across any row is one cycle of the eruption, stretching, and finally breaking of the flame envelope - the pulsation or oscillation associated with large diffusion flames. Eight frames per cycle corresponds to a period of about one-third second. If the length of the intermittent region, $(0.20 - 0.08)$ m kW$^{-2/5}$, is divided by the period, the velocity of flame travel will be obtained. (This is the

flame movement as viewed in a picture, not a flame propagation velocity).
For the data here this number ranges from 1.1 to 1.8 m/s. From table 1 the
gas velocity in the intermittent region ranges from 3.3 m/s to 4.3 m/s, a
factor of 2-1/2 to 3 times larger. Hence measurements based on photographing
flame travel will be considerably low [12]. (For the buoyancy constant, C,
0.9/0.36 = 2-1/2. The constant 0.36 is an often quoted literature value.)
For a non-luminous flame the intersection of the two lower flame regimes
may be visually quite indistinguishable. The inward necking or pinching
and separation from the anchored fuel-rich core near the burner may be
difficult to observe without the naturally occurring soot "tracer" seen in
the present photographs (see reference 16).

A comparison of the present data with some previous work is shown on
table 2. Only the plume region has been investigated to any extent with
the exception of Heskestad's work whose measurements extended into the
flames. The results are presented in terms of a source buoyancy rate
parameter [9], $F_o = gQ/\rho_o c_p T_o$. Note the third column is independent of heat
release rate, Q, whereas the fourth column is independent of distance from
the source. This is a result of some practical importance and is discussed
in detail by Heskestad who has collected data for a large range of fire
sizes, Q = 40-25000 kW. The present results indicate that $V/(Q\Delta T)^{1/5}$
ceases to be a constant in the intermittent regime and is a function of z
equal to $(1.93/62.9^{1/5} = 0.843)$ or $0.843 (z/Q^{2/5})^{1/5}$ (see table 1). Between
the two intersections, $z/Q^{2/5} = 0.08$ to 0.2 m $kW^{-2/5}$ $V/(Q\Delta T)^{1/5}$ will rise
from 0.51 at the flame-intermittent intersection to 0.61 in the plume.
Perhaps the low value, 0.50 of reference 3 represents some kind of average
of both plume and intermittent data.

The present data are most like those of Yokoi, falling about 5% lower
in velocity and 12% lower in temperature. One major difference between the
two experiments is flame radiation – alcohol burns with little soot radiation
while the present gas flame was very luminous. Significant flame radiation
could decrease the amount of energy available for buoyancy in the plume.
Since V and ΔT depend on heat release rate differently it is possible to
estimate the effective or buoyancy component of Q: comparing Yokoi and the
present results from table 2 $(3.7/3.9)^3 = 0.85$ and $(8.0/9.1)^{3/2} = 0.82$.
(Note that a small increase in $\Delta T z^{5/3}/Q^{2/3}$ from table 1 could bring the
reduction in Q up to 0.85. Recall that the mean values in table 1 are
weighted in favor of the smallest fire where center line temperature errors
due to radiation are suspected to be largest.) This indicates that in the
order of 15 to 20% of the heat release is lost in the form of flame radiation
in the present experiments and does not contribute to buoyancy. Note that

Yokoi's temperature data has recently been confirmed by Zukoski [10] for a completely premixed flame system and hence the data of reference 8 appears to be high. The value of 20% appears reasonable for a radiative component for this system. Reference 11 presents measurements which yield, for a simple pipe burner, radiation loss of 3.3 kW/SCFM of CH_4 (1 CFM = 0.472 l/s) and hence 3.3/(0.472 x 35) = 0.2. Obviously much more detailed analysis of flame radiation including RMS volume and absorptivity measurements are required for more precise calculations.

3.2 Radial Variation of the Data

Horizontal traverses of time-averaged V and ΔT were made at various heights above the burner spanning the three vertical regimes for two different heat release rates, Q = 22 and 45 kW. With the exception of perhaps the plume no single line through the data was judged to be an adequate fit to a Gaussian representation of the data using x^2 or $x^{3/2}$ as independent variables. As x increases away from the center line (bulk of flames) the data would fall above a line determined by the near center data.

In order to obtain first a broad view of the spreading of the fire the width where the velocity falls to 1/e of the value on the center line $(x_{1/e})$ was determined at each height. This was accomplished by interpolation of a faired line through the data since no single analytical characterization using all the data for a single traverse could be found, i.e., $x_{1/e}$ will be heavily weighted by the data in the "wings". On a plot of the width, $x_{1/e}$ vs the height, z, no recognizable difference between the flame and the intermittent regime was apparent due to the considerable scatter in the data. So both regimes were lumped into one and a linear least squares fit of $x_{1/e}$ vs z was made for both sets of heat release data. The results indicate that the larger fire has a larger $x_{1/e}$ intercept, i.e., wider base, and a smaller slope, i.e., it does not spread as rapidly, as compared to the smaller fire. From the center line analysis the appropriate scaling for height was determined to be $z/Q^{2/5}$. If that length scale is used the linear fit can be expressed as $x_{1/e} = mz/Q^{2/5} + b$ for both sets of data. In this form the values of the two slopes, m, turn out to be remarkably similar, within a few percent. This would indicate that the spread rate is independent of heat release in the scaled coordinate and depends only on Q through the initial width.

The intercept or initial width, b, at the same time, comes out to be a function of Q to very close to the 1/2 power. This is an important result since most materials burning under the influence of their own flame radiation

will exhibit a constant burning rate per unit area, the so-called burning velocity. That is, except for small samples, the larger the sample area the greater the heat release rate, and $Q \sim A_o \sim x_o^2$, where x_o is a characteristic dimension of the source. Yokoi proposed for finite area sources the scaling relation between the radius of the source, r_o and the strength of it as: Q/r_o^2 and then showed by comparing data in the plume region for alcohol lamps its validity for sources larger than about 10 cm. Terai has flame height varying with $r_o^{4/5}$ for methanol pool fires. The present intersections, $z \sim Q^{2/5}$, will also follow $x_o^{4/5}$ if $Q \sim x_o^2$.

The present results, $x_{1/e,o} \sim Q^{1/2}$ and slope $\sim Q^{-2/5}$, means a smaller fire starts from a smaller area but diverges at a faster rate than a larger fire, perhaps because the smaller fire has less buoyancy generated momentum in the wings. This result in fact may be more general than the use of a single sized burner might indicate. Here heat release ranged from 15 to 60 kW which corresponds to about 150 to 600 kW/m^2. This value for given circumstances is fixed for a given material and depends on a multitude of parameters. Cellulosics range from about 100 to 200 kW/m^2; for ethyl alcohol it is about 650 kW/m^2, and a commonly studied polymer, PMMA, is about 530 kW/m^2 for a large pool. Instead of using different materials in different sizes which should yield, if the sample is large enough, similar results, since the burning rate per unit area is constant, the burner can simulate different materials of a similar size by changing the gas flow or heat release rate. The flame shape above the burner appears to neck down for small flow rates and to broaden for higher flows. Obviously the partition of radiative and convective energy will vary from material to material and hence care must be exercised in interpretating the present results.

The radial results can be seen in figure 5 which is a plot of $x_{1/e}$ vs $z/Q^{2/5}$ for the two fires. The solid lines through the data are the least squares fit discussed above and only include the points in the flame and intermittent regime. It is doubtful whether the lines are valid as drawn on the figure very close to the surface of the burner since flow asymmetry may begin to dominate here. Also some necking of the flow may be occurring as seen on the flame photographs (figure 3). Recall that the time-averaged results will include flame as well as cold entrained air passing the probes. Since both sets of points yield the same slope the question arises about the statistical significance of having two lines. By subjecting the intercepts to Student-t statistics and also comparing two standard deviation bands around the intercepts it can be shown that the lines are indeed distinct. Note that it is not possible to obtain a single universal curve of the width data as was done for the vertical direction data in terms of heat release rates due to the area dependence of Q.

12

The plume data which horizontally appears moderately self similar is
shown by dashed lines originating from the center of the surface of the
burner. Recall that for distances far enough away from the source a plume
will behave independently of the source. The slopes, $x_{1/e}/z$, of the five
plume points average 0.195 with a scatter of $\pm$ 6% which corresponds to an
entrainment constant, α = 0.195 x 5/6 = 0.16, a rather high value. As
expected these values are independent of Q and will therefore not fall on a
single curve in a $z/Q^{2/5}$ coordinate. Note that if the plume were not
totally developed and the five points were included in the least squares
analysis performed previously the conclusions reached there will not be
very different, that is, $x_{1/e,o} \sim Q^{1/2}$ and slope $\sim Q^{-2/5}$.

In terms of a virtual source, a position where the flow originates
below the burner, the distance will be almost a linear function of Q, the
exponent equal to 0.9. In this framework the entrainment coefficient (5/6
times the slope) for the flame-intermittent regime would be about 0.15 for
the smaller fire, decreasing to 0.10 for the larger fire. The numbers will
shift slightly if the plume points are included but the tendency for lowering
of α with increasing fire size will remain.

The plume radial data is shown on figure 6 where the velocity V at any
width x is plotted in similarity form, V/V_o vs x/z, where V_o is the center
line value and z is the height above the burner. The lines represent a
Gaussian distribution with three different entrainment coefficients which
bracket most of the data. With the considerable amount of scatter present
the futility of identifying a particular entrainment coefficent unequivocally
is obvious.

Figure 7 shows the intermittent velocity data where the x coordinate
has been normalized by the least squares expression for $x_{1/e}$, not the indi-
vidually determined values. With considerably more data than in the plume
regime the results appear to exhibit less scatter. An appropriate repre-
sentation of the data might be the function $\exp[-(x/x_{1/e})^{3/2}]$. There is not
a great deal of difference between the overall shape of the decaying
exponential function using 3/2 as opposed to 2 as the power of x. The
former will decay more quickly for values of $x < x_{1/e}$ and will decrease less
rapidly for $x > x_{1/e}$ a tendency noted in both the intermittent and flame
data. Yokoi actually proposes a 3/2 expression multiplied by a power
series of x/z for the distribution of velocity and temperature.

Finally, figure 8 presents the flame region velocity data. The scatter
is considerable. Near the center line the data indicate that a less rapidly

13

decaying function, e.g., $(x/x_{1/e})^2$ would be more appropriate. In the wings
the opposite condition is indicated, i.e., 3/2 is too large. The data near
the center line and close to the burner show the same tendency as the center
line data did previously, i.e., the velocity and temperature in the fuel-
rich region fall below the tendency shown by data further away from the
burner. Likewise here when one moves horizontally away from the center line
into a more uniformly mixed region, V and ΔT rise above the center line
values before falling. This would be similar to probing the flame sheath
of a high velocity diffusion flame where the boundary of fuel and air is
sharply distinct.

In the flame and the intermittent region to some extent there is
confusion as to the shape of the profile in the wings. For example, on
figure 8 for z = 0.287 (filled squares) the velocity falls away from the
center line up to $x/x_{1/e}$ = 0.86. The next data point, $x/x_{1/e}$ = 1.03 is
actually at a higher velocity than the previous points. This is an exag-
gerated case but, in this region, there is a tendency for the curve to
"flatten out" before falling. That is, the velocity (and temperature)
remains nearly constant for a short radial distance before decreasing. It
is not clear if this phenomenon is associated with the large-scale eddy
motion seen at the edges but perhaps it might shed some light upon the
mixing process since these are long time averaged results. At present it
makes the determination of a distinct width parameter, $x_{1/e}$ in this region
difficult.

In order to remove some of the arbitrariness of the above data
interpretation a numerical scheme was applied to the radial data. It consisted
of assuming that the data follows a decaying exponential, i.e., V/V_o =
$\exp[-(x/x_{1/e})^n]$ whose n and $x_{1/e}$ are unknown. By taking logarithms twice a
linear least squares fit could be made of the data yielding both n and $x_{1/e}$
at each vertical position. The determined n was interesting. Near the
burner n was approximately 2.5 (indicative of the high values just off the
center line seen in figure 8) and fell with z to approximately 1.5 at the
start of the intermittent regime. In the plume it rises with z from 1.5 to
about 2 for the large z points. The values of $x_{1/e}$ were not very different
from those obtained by visual interpolation except for some distortion
noted near the burner surface resulting from the "flattened" profiles noted
above. These results indicated that the previous data handling is probably
sufficiently accurate for the present overall view of the fire.

The temperature rise distribution in the radial direction is very
similar to the velocity distribution. If temperature rise at any x is

14

normalized by the center line value and plotted as in figures 6, 7, and 8 the results will be similar to the velocity results shown on those figures with one exception. Throughout the three regimes and for both fire sizes the velocity profile is wider than the ΔT profile. By finding the $1/e$ value of the temperature rise distribution as was done for the velocity distribution the two widths can be quantitatively compared. The mean for all values at each height and fire size yields $(x_{1/e})_V / (x_{1/e})_{\Delta T} = 1.2$ with a standard deviation of 0.13. The difference in the widths is more or less uniform throughout the plume and intermittent regime and becomes somewhat less (~ 1.1) in the flame region. Thermocouple radiation error may be most severe in the wings of the flame regime causing high readings and thus appearing to bring the temperature profile close to the velocity profile.

The fact that the velocity profile turns out to be wider than the temperature is contrary to the classical plume results [8] but recent work by George et al. in the plume region of a heated jet also has $(x_{1/e})_V / (x_{1/e})_{\Delta T}$ greater than one. There it was equal to 1.09 for a limited number of measurements. Also Terai finds the ratio to be about 1.3 for methanol pool fires of this size. Plumes along walls also exhibit this behavior.

Since, on the center line, the buoyancy relation $C = \dfrac{V}{\sqrt{2gz\Delta T/T_o}}$, is remarkably consistent throughout the three regimes it will be worthwhile to investigate its off-axis behavior in the radial direction. It might be possible to estimate the loss of z-direction momentum to large-scale mixing in the wings. The plume results of Rouse et al. can be recast in terms of the buoyancy constant as:

$$C = \frac{4.7}{\sqrt{2 \times 11}} \quad \frac{\exp\left(-96\,\frac{x^2}{z^2}\right)}{\exp\left(-1/2 \times 71\,\frac{x^2}{z^2}\right)} = 1.0 \exp\left(-60.5\,\frac{x^2}{z^2}\right)$$

and for George et al. [9]:

$$C = \frac{3.4}{\sqrt{2 \times 9.1}} \quad \frac{\exp\left(-55\,\frac{x^2}{z^2}\right)}{\exp\left(-1/2 \times 65\,\frac{x^2}{z^2}\right)} = 0.80 \exp\left(-22.5\,\frac{x^2}{z^2}\right)$$

For ease of comparison the previous expressions can be given in terms of an actual width, the $x_{1/e}$ value of the various distributions, e.g., $x_{1/e}{}_V = \dfrac{1}{\sqrt{96}}\, z = 0.102\, z$, etc. Also let the width of the C distribution be $x_{1/e}{}_C$. From the definition of C and the assumed exponential profiles

$$\frac{x_{1/e\,C}}{x_{1/e\,V}} = \left(\frac{1}{1 - 1/2\left(\frac{x_{1/e\,V}}{x_{1/e\,\Delta T}}\right)^n} \right)^{1/n}$$

where n is the exponent of the width scale, x, in the exponential which is equal to 2 in the expressions above. This will give an idea of how closely the decay in buoyancy follows the decay in velocity. The present results are compared with the previous two references in the following:

	$\dfrac{x_{1/e\,V}}{x_{1/e\,\Delta T}}$	$\dfrac{x_{1/e\,C}}{x_{1/e\,V}}$
YIH	1/1.16	1.3
George	1.09	1.6
Present	1.2	1.9 n = 2
		2.0 n = 3/2

It appears then that the decay in C is significantly less than the decay in velocity, the C profile being about twice as wide. Any radiation error will tend to bring C closer to V but the high value for reference 9 where no flame was present tends to indicate that more exact radiation corrections would not alter this conclusion. Note the limits on $\dfrac{x_{1/e\,C}}{x_{1/e\,V}}$ for various $\dfrac{x_{1/e\,V}}{x_{1/e\,\Delta T}}$. The upper limit, $C \neq C(x)$, i.e., $x_{1/e} \to \infty$ is for $\dfrac{x_{1/e\,V}}{x_{1/e\,\Delta T}}$ equal to $2^{1/n}$, e.g., 1.4 for n = 2. Going the other way, $\dfrac{x_{1/e\,V}}{x_{1/e\,\Delta T}}$ decreasing through 1 (reference 8) toward 0, $\dfrac{x_{1/e\,C}}{x_{1/e\,V}}$ approaches 1, the decay rate of C approaches that of velocity.

Instead of plotting ΔT in the x direction for the three regions which will be virtually identical to the velocity figures 6, 7, and 8, except for the smaller width, it might be more instructive to plot isotherms in actual space coordinates, z vs x. Figures 9 and 10 do this for both fire sizes. The x-axis is greatly exaggerated (5x) so that the detail at the base of the burner can be distinguished. The dots on the figures are interpolated values at hundreds of degrees, the curves are simply faired representations through the dots. Interpolated values from the center line scanning are also shown by dots on the ordinate. The three vertical regimes are marked on the figures. For the larger fire, figure 10, the fuel-rich region near the base of the burner characterized by lower ΔT close to the center line can be clearly distinguished. The maximum temperature occurs some distance

16

from the origin. For the smaller fire it would probably take a traverse
closer to the face of the burner before this behavior could be seen.

Comparing figures 9 and 10 to figure 3 which shows the 1 s time
exposed photographs, it is possible to sketch the visible flame envelope.
For the smaller fire (figure 9) the envelope will nearly coincide with an
isotherm of about 320 - 350° C starting from the center line down to a
height of about 0.2 m. Below this height it begins to bend across the 300
and 200° C isotherms approaching the burner edge at the surface. The
larger fire shows similar behavior except the envelope crosses through
higher temperature regions midway down toward the surface. With the increased
scatter on figure 10 it is difficult to draw conclusions about this behavior.

3.3 Effect of Floor and Ceiling

In order to investigate the effect of locating the burner surface
flush with a floor, a noncombustible sheet was placed around the burner
edge for a distance of one burner width (W) on all sides. The entire
square had dimensions then of 3 W x 3 W. The entrained flow field would
conceptually be completely different than the previous configuration where
the burner could suck flow from below and up along the sides of the burner.
With the simulated floor in place this vertical flow would be cut off and
air would be required to come in horizontally before turning upward into
the flame.

Figure 11 shows the result of center line traversing with the floor in
place, the points representing two fire sizes and the lines represent the
previous correlations for no floor. There are some differences, notably
the flame temperatures appear slightly higher and plume temperatures slightly
lower, with velocity differences in the same directions. However, in
general, these differences are slight for such a radical change in con-
figuration. A few radial scans were made with the "floor" in place and
like the center line no significant changes were recorded. The radial
scatter, though, is considerable in any case.

One noteworthy observation concerns the stability of the floor
configuration. The flame was much more sensitive to disturbances than when
there was no floor. With the floor in place if one walked by the burner at a
pace and distance that would not noticeably disturb the flame in the normal
configuration, the flame was apt to behave wildly, leaning far to one side
with a tendency to form fire whirls at one of the corners of the burner.
After some time in the absence of further disturbance the flame would again
become symmetric.

Also in the spirit of looking for gross effects, a 1 m^2 noncombustible sheet was placed horizontally and centrally above the burner to simulate the effect of a ceiling on the fire, i.e., to evaluate any far field elliptic characteristics. Again the results were not affected at least as regards the center line behavior up to a height of about 70% of the height of the ceiling.

3.4 Nature of the Signals

In order to obtain the overall gross structure of a typical diffusion flame analysis up to this point has involved time-averaged quantities. Long-time integration has masked naturally occurring pulsations, turbulence, or ambient disturbances. In order to try to understand the gross structure more detailed information will be required. Cox has investigated thermal and electrostatic probe fluctuations for this flame system and in this section the nature of the pressure signal which is related to velocity fluctuations will be described. Recall that the probe volume is considerable so fine scale information will not be sensed but rather the macroscopic structure of the flame may be further elucidated.

Figure 12 shows the unprocessed dc output of the electrical manometer on a fast-writing recorder (through an oscilloscope the signal appears identical). This record is from the center line at the upper edge of the flame region. Within the vertical lines, corresponding to a 1 s time interval, periodic activity of approximately 3 Hz can be observed consistently. The size of the fluctuations are not trivial and the need for conditioning in determining the time-averaged velocity behavior is obvious. To the left of the unprocessed signal is shown the result of conditioning through an integrating voltmeter for an averaging time (τ) of 100 s. For the center line all but the very low frequencies associated with large laboratory disturbances are eliminated for even smaller averaging-time settings, i.e., $\tau = 10$ s and 1 s. In the wings however, activity still persists at higher τ's as the fire sways about. The average dc level is about 1.9 volts. (The question of instrument frequency response will be addressed below.)

The same signal was also passed through a true root mean square (RMS) meter with variable high pass filters on the input. The dc is thus removed so the resulting RMS is essentially a standard deviation measurement. With the meter set for acceptance of the lowest possible frequency range, i.e., $f > 0.1$ Hz the RMS pressure value determined was 0.0073 torr at a dc level of 0.019 torr or $\sqrt{\overline{\Delta p'^2}}/\overline{\Delta p} = 0.38$. For higher minimum frequency settings of

the meter the RMS value decreases indicating that most of the energy is at low frequencies. Note that since these are high pass filters the upper end of the frequency spectrum is unaffected by minimum frequency cutoff.

Also on figure 12 is the auto-correlation function for a similar center line signal. The auto-correlation function compares or correlates a given signal with a delayed version of itself for different delay time, (τ_a) the abscissa on the photo in figure 12. At τ_a = 0 the two signals are obviously most similar and the ordinate is the mean square value of the signal. In this case $\Delta p'^2$ = 0.00005 torr^2 or $\sqrt{\Delta p'^2}$ = 0.0071 torr, similar to the voltmeter result. The useful property of correlation here is the fact that the auto-correlation function of a periodic signal is periodic and has the same period as the signal. Hence the raw signal seen in the unprocessed chart recorder plot on the lower part of figure 12 can be interpreted not as random noise but as a repetitive signal of period approximately 0.33 s. Where the auto-correlation function goes to a maximum, i.e., τ_a = 0.33, 0.68, etc. on the picture the signal is most like itself. For longer and longer delay times the amplitude of the correlation function will decrease at each of the maxima due to finite statistics and deviations from a pure sinusoid, i.e., broadening of the spectrum. The number of samples for the 100 point trace shown was 8 x 1024.

Taking the Fourier transform of the auto-correlation function leads to its equivalent in the frequency domain, the power density spectrum. Figure 13 (provided by Cox) is a plot for a similar Δp signal of the relative power spectrum (maximum equals 1) and the amount contained at each frequency interval, seen in the lower linear trace for the frequency range of 0.5 to 50 Hz. During the previous discussion concerning the RMS results it was determined qualitatively that most of the energy appeared to be at lower frequencies. Figure 13 gives a quantitative answer to the energy distribution question. The dominance at 3 Hz (or slightly less) is quite unequivocal in both plots. A second two decade scan from 5 to 500 Hz shows similar results as that seen in the figures up to 50 Hz. Unfortunately there appears to be an instrument response problem at about 20 Hz (the 5 to 500 Hz scan exhibits another at 40 Hz). Determination of frequency response for a transducer-tubulation (probe, tubing, valves, manometer) system like the present is not a simple matter [13] and without further information detailed interpretation of figure 13 would be of questionable value. Fortunately Cox has obtained spectra for $\Delta T'$ for this burner at similar conditions and that result is practically identical (except for the sharp attenuation at 20 Hz) to figure 13 thus strengthening somewhat the contentions about the low frequency activity.

The 3 Hz frequency is a factor of three lower than the classical results for oscillations or "flame flicker" of laminar diffusion flames such as candle flames. These have been found to be always of the order of 10 Hz and are unaffected by the dimensions or type (including square) of burner, the fuel flow rate or fuel type [14].

On the other hand, in a study of large-scale diffusion flames McCamy [15] measured flicker frequencies optically and found peak amplitudes at frequencies between 3 and 10 Hz. These were sharp maximums with peaks 100 times the average amplitude over the range from 2.5 to 750 Hz. Diffusion flames over lubricating oil and hydraulic fluid contained in a 0.15 m diameter pan yielded precisely 3 Hz. A natural gas diffusion flame above a small burner exhibited a peak at slightly less than 5 Hz. Like the 10 Hz results above, the initial momentum may not be negligible due to the small size of the burner and hence the flames may not be truly buoyant. For this case the flicker was so regular that second and third harmonics were detectable. A gasoline diffusion flame exhibited two peaks of similar magnitude at 5 and 8 Hz. A further summary discussion of flame oscillations can be found in reference 16 where a variation of frequency with pool size has been observed for methanol fires. The present 3 Hz result is not inconsistent with those findings for similar size pools. (Terai also finds peaks at about 3–4 Hz in his power density spectrum of temperature fluctuations.)

How this fluctuating structure varies throughout the flame can be seen on figure 14 where the voltmeter RMS reading (f > 0.1 Hz) is plotted along with the dc component and also the ratio of the two. The upper portion of the figure gives center line results throughout the three regimes. From the base of the burner to well into the plume region $\overline{\Delta p}$ and $\sqrt{\overline{\Delta p'^2}}$ vary by almost an order of magnitude and yet the ratio of the two remains virtually constant at about 0.35. Judging by the voltmeter results with the variable high pass input filter the frequency distribution is probably similar to figure 13 everywhere. That is, a spectrum analysis was not obtained at each and every point of figure 14 but the RMS voltmeter was used at three minimum frequency cutoffs during those traverses and the lower frequency dominance was maintained throughout. The 3 Hz frequency then is something fundamental throughout the entire flame to plume structure and the ejection of flame "tongues" in the intermittent region is just one manifestation of the phenomenon.

The radial scan at z = 0.267 m, near the tip of the flame region shown on the lower portion of figure 14, is more interesting regarding this behavior. The time-averaged signal falls with radial distance, x, as was seen previously

20

in the velocity profiles. The fluctuating components on the other hand decrease much less with distance into the wings. The net result is that the ratio of the two signals starts at about 0.35 at the center line and increases radially until at the extremities the RMS almost constitutes the entire signal. The RMS portion has not changed very much throughout x, but $\overline{\Delta p}$ representing a net upward flux, decreases such that at the extremes there is no longer a preferred upward tendency. It is this lack of strong direction coupled with significant fluctuations that makes the wing measurements difficult. Note again that these are large-scale pulsations and make the truly buoyant diffusion flame subject to even minor ambient disturbances.

3.5   Entrainment and Heat Release

The mass flow rate, m, at any height above the burner assuming axial symmetry is given by:

$$m(z) = \int_{0}^{\infty} \overline{\rho v}(z,x) \; 2\pi \; x \; dx$$

Since any correlation between ρ and v is presently not well understood for these systems it will be assumed that $\overline{\rho v} = \overline{\rho} \times \overline{v}$. Using an ideal gas with

$$\Delta T(z,x) = \Delta T(z) \; \exp[-(x/x_{1/e})^2]$$

$$V(z,x) = V(z) \; \exp[-(x/x_{1/e})^2]$$

the mass flow rate expression can be easily integrated. The exponent 2 was chosen as well as a single characteristic width, $x_{1/e}$ for both the velocity and temperature profiles in order to obtain a perfect differential. Mass flow becomes:

$$m(z) = \pi \; \rho_o (x_{1/e_V})^2 \; \frac{V(z)}{\Delta T(z)/T_o} \; \ln \left(\frac{\Delta T(z)}{T_o} + 1 \right)$$

Note that if $x_{1/e}$ was used as an upper limit of integration instead of ∞ the ln term would become slightly more complex leading to a significant reduction in mass flow rate, e.g., a factor of two in the flame region. This is because although velocity is getting smaller density is getting larger, approaching ambient, and hence $\overline{\rho v}$ is not falling as rapidly as v. The integration limits are therefore important. This is in contrast to constant density flows where there is a smaller fraction of flow from $x_{1/e}$ to ∞.

21

The equation for m(z) states that the mass flow rate is basically the cold density times the area within x_{1/e_v} times the center line velocity. The modifying factor of temperature, i.e., $\frac{\ln(\Delta T/T_o + 1)}{\Delta T/T_o}$ accounts for the variable density. Far into the plume with $\Delta T \to 0$ the factor equals 1.0. Toward the other extreme in the flame the factor equals about 0.5 and hence the mass flow is almost independent of temperature and consequently it is not so sensitive to radiation error in the thermocouple measurement.

Substituting for V and $\overline{\Delta T}$ into the expression for m yields

$$m(z) = C_1 (x_{1/e_v})^2 \, Q^{1/5} \, \left(\frac{z}{Q^{2/5}}\right)^{1-\eta} \ln \left[C_2 \left(\frac{z}{Q^{2/5}}\right)^{2\eta-1} + 1 \right]$$

$$\text{where } C_1 = \frac{2g\pi\rho_o c^2}{k} \quad \text{and} \quad C_2 = \frac{(k/C)^2}{2g}$$

$$\text{and } x_{1/e_v} = \alpha \, \frac{z}{Q^{2/5}} + \beta \, Q^{1/2}$$

values of k and η are given previously for the three different regimes. C is constant throughout and due to the limited amount of plume data α and β can also be considered constant throughout. Figure 15 shows the resulting flow rate, m, of the above calculation plotted against normalized height above the burner for various fire sizes. A useful simplifying expression valid in the near field is:

$$m = 0.055 \, z \, Q^{1/2} \, [\text{kg. s}^{-1}] \quad z[\text{m}], \, Q \, [\text{kW}]$$

which states that the flow rate is proportional to the height above the burner to the first power and depends on heat release rate to a significant degree. Both of these effects are missing in most formulations based on plume theory [5]. Of course, in the above expression x_{1/e_v} for the flame and intermittent region was used in the plume due to limited plume data and hence these results will not be valid far away from a small fire where plume theory will apply, i.e., m will be a stronger function of z and a weaker function of Q.

The convective energy flux at any height for a given fire size is:

$$H(z) = C_p \int_0^\infty \overline{\rho V} \, \Delta T \, 2\pi \, x \, dx$$

Using the same assumptions as before, namely: the time-averaged of the product is equal to the product of the time-averaged quantities, and a square power Gaussian for both V and ΔT having equal widths. The integration results in:

$$H = \pi \, C_p \, \rho_o \, (x_{1/e_{\Delta T}})^2 \, V(z) \left[\frac{\Delta T - T_o \ln\left(\frac{\Delta T}{T_o} + 1\right)}{\Delta T / T_o} \right]$$

or comparing to the equation for mass flow:

$$H = \frac{m \, C_p \, T_o}{(1.2)^2} \left[\frac{\Delta T / T_o}{\ln\left(\frac{\Delta T}{T_o} + 1\right)} - 1 \right]$$

Note that for H, $x_{1/e_{\Delta T}}$ is chosen as the appropriate width since the multiplication by ΔT which falls much faster than ρV will control the H profile. For mass flow x_{1/e_V} was used since ρV was on the wider side of either the ΔT or V profile.

Figure 16 shows the convective energy flux normalized by the nominal heat release rate, H/Q, plotted against $z/Q^{2/5}$. Since Q is the energy originally supplied to the burner H/Q indicates how much energy is realized convectively and therefore cannot exceed 1.0. Previously it was estimated that 15 to 20% of Q is radiated away in the luminous zones so perhaps more realistically H/Q cannot exceed about 0.8. Except for the very small fires H/Q reaches about 0.55 independent of Q at the flame-intermittent inter-section. In the intermittent regime for the larger fires H/Q rises weakly or not at all. Thereafter, in the plume region H/Q begins to fall as combustion ceases and dilution begins to dominate. The results for the majority of the present data, i.e., 20 to 50 kW envelop a region around 0.8 at the top of the intermittent regime indicating roughly the validity of the previous experimental results and the above analytical approximations. Although there may exist some tendency for radiation to increase with fire size and hence result in lower H/Q the high values (H/Q $\geq$ 1) for the small fire point out the need for further refinement. Extrapolation to Q below the range of measurements will lead to errors due to the form of $x_{1/e}$, i.e., the first term, $\alpha \, z/Q^{2/5}$, will begin to dominate.

23

4. SUMMARY AND CONCLUSIONS

A pressure probe and thermocouple have been used to determine the near field characteristics of a buoyant, area source, diffusion flame. The validity of this technique, for velocity measurement in <u>buoyant</u> flames appears to be demonstrated. This contention is based on agreement with previous measurements in the less severe plume region where different instruments, e.g., hot wires have been utilized. There is also consistency between the present results and a number of cross correlation measurements in the flame regime.

The results of center line probing have established the time-averaged fluid mechanical and thermal fields or gross structure of the flame. In addition the scaling relations in terms of a nominal heat release rate, i.e., $V \sim Q^{1/5}$ and $z \sim Q^{2/5}$ have been established. The measured demarkation of the fire into flame-intermittent-plume regimes as well as the visual identification of each have been seen to characterize the phenomena. The dominant role played by buoyancy is shown by the consistency of $V/\sqrt{2gz\Delta T/T_o}$ in all three regimes.

A tentative scaling for width, $x_{1/e} \sim \alpha\, z/Q^{2/5} + \beta\, Q^{1/2}$ has been proposed and it is in this area that definite further study is required. More refined radial scanning of different sized burners/pool fires will be necessary in order to demonstrate proper scaling.

Having found the center line and radial behavior of the flame system, expressions for mass entrainment and heat release were determined. Assessment of H/Q can provide a simple check of overall accuracy.

Additional experiments should include an evaluation of radiation from the flames. Various methods are available whereby the total radiative power output of the flame can be ascertained with a minimum of straightforward flux measurements.

Finally, on the analytical side, information like the dominance of 3 Hz and future finer scale spectral measurements, especially in the mixing regions, can provide guidelines for modeling characterization.

5. ACKNOWLEDGEMENTS

6. REFERENCES

[1] Cox, G., to be published.

[2] Terai, T., Experiments on Plume Rising from Burning Heat Source with Finite Sizes, to be published.

[3] Heskestad, G., Optimization of Sprinkler Fire Protection Progress Report No. 9, Factory Mutual Research Corporation, Norwood, Mass., March 1974.

[4] Yokoi, S., Study on the Prevention of Fire-Spread Caused by Hot Upward Current, Report of the Building Research Institute, Ministry of Construction, Japan, No. 34, Nov. 1960.

[5] McCaffrey, B. J. and Rockett, J. A., Static Pressure Measurements of Enclosure Fires, Journal of Research of the National Bureau of Standards, 82^2, 107 (1977).

[6] McCaffrey, B. J. and Heskestad, G., A Robust Bidirectional Low Velocity Probe for Flame and Fire Application, Combustion and Flame 26, 125 (1976).

[7] Thomas, P. H., Baldwin, R. and Heselden, A. J. M., Buoyant Diffusion Flames: Some Measurements of Air Entrainment, Heat Transfer, and Flame Merging, Tenth Symposium (Int.) on Combustion, The Combustion Institute, 1965, pp. 983-996.

[8] Rouse, H., Yih, C. S. and Humphreys, H. W., Gravitational Convection from a Boundary Source, Tellus 4, 201 (1952).

[9] George, W. K., Alpert, R. L. and Tamanini, F., Turbulence Measurements in an Axisymmetric Buoyant Plume, Factory Mutual Research Technical Report No. 22359-2, Norwood, Mass., Jan. 1976.

[10] Veldman, C. C., Kubota, T. and Zukoski, E. E., An Experimental Investigation of the Heat Transfer from a Buoyant Gas Plume to a Horizontal Ceiling, Nat. Bur. Stand. (U.S.), NBS-GCR-77-97 (1975).

[11] Powers, R. M., Calorimetry of Luminous Natural Gas Flames, 2nd AIAA/ASME Thermophysics and Heat Transfer Conference, Palo Alto, Calif., May 1978.

[12] Thomas, P. H., The Size of Flames from Natural Fires, Ninth Symposium (Int.) on Combustion, The Combustion Institute, 1963, p. 844.

[13] Iberall, A. S., Attenuation of Oscillatory Pressure in Instrument Lines, Research Paper RP 2115, Journal of Research of the National Bureau of Standards, 45, 85 (1950).

[14] Grant, A. J. and Jones, J. M., Low-Frequency Diffusion Flame Oscillations, Combustion and Flame 25, 153 (1975).

[15] McCamy, C. S., A Five-Band Recording Spectroradiometer, Journal of Research of the National Bureau of Standards, 56^5, 293 (1956).

[16] Hertzberg, M., Cashdollar, K., Litton, C. and Bugess, D., The Diffusion Flame in Free Convection, U.S. Bureau of Mines Report RI 8263 (1978).

[17] Beuther, P. D., Capp, S. P., George, W. K., Momentum and Temperature Balance Measurements in an Axisymmetric Turbulent Plume, American Society of Mechanical Engineers Paper No. 79-HT-42 (1979).

Table 1. Summary of center line data

Fire Size	Q(kW)	14.4	21.7	33.0	44.9	57.5	Weighted Average
Flame	ΔT (°C)	791	800	807	790	800	797
	$V/z^{1/2}$ ($m^{1/2} s^{-1}$)	6.87	6.83	6.89	6.77	6.80	6.84
	$\dfrac{V}{\sqrt{\dfrac{2g\Delta Tz}{T_o}}}$	0.943	0.932	0.936	0.930	0.928	0.936
		(22)	(11)	(8)	(12)	(8)	(61)
Intermittent	ΔTz (°C m)	171	221	277	326	353	
	$\Delta Tz/Q^{2/5}$ (°C m $kW^{-2/5}$)	58.8	64.5	68.4	71.2	69.8	62.9
	V (ms^{-1})	3.29	3.59	3.92	4.10	4.24	
	$V/Q^{1/5}$ ($ms^{-1} kW^{-1/5}$)	1.93	1.94	1.95	1.92	1.89	1.93
	$\dfrac{V}{\sqrt{\dfrac{2g\Delta Tz}{T_o}}}$	0.971	0.932	0.909	0.877	0.871	0.940
		(39)	(10)	(5)	(10)	(5)	(59)
Plume	$\Delta Tz^{5/3}$ (°C$m^{5/3}$)	122	166	240	314	357	
	$\Delta Tz^{5/3}/Q^{2/3}$ (°C$m^{5/3} kW^{-2/3}$)	20.6	21.3	23.3	24.9	24.0	21.6
	$Vz^{1/3}$ ($m^{4/3}s$)	2.72	3.10	3.61	3.98	4.12	
	$Vz^{1/3}/Q^{1/3}$ ($m^{4/3}s^{-1} kW^{-1/3}$)	1.12	1.11	1.13	1.12	1.07	1.12
	$\dfrac{V}{\sqrt{\dfrac{2g\Delta Tz}{T_o}}}$	0.951	0.929	0.900	0.867	0.842	0.928
		(27)	(8)	(4)	(4)	(3)	(46)
	$V/\sqrt{\dfrac{2g\ \Delta Tz}{T_o}}$ All Q All z						.935 (176)

		ΔT			V		
	Flame-Intermittent	$\dfrac{62.9}{797} = .0789$			$\left(\dfrac{1.93}{6.84}\right)^2 = .0796$		.0793
Intersections $z/Q^{2/5}$ ($m \cdot kW^{-2/5}$)	Intermittent-Plume	$\left(\dfrac{21.6}{62.9}\right)^{3/2} = .201$			$\left(\dfrac{1.12}{1.93}\right)^3 = .195$		.198

( ) number of data points

27

Table 2. Comparison to previous work, plume,
center line-axisymmetric

	Velocity $V = A F_o^{1/3} z^{-1/3}$		Temperature Rise $g\frac{\Delta T}{T_o} = B F_o^{2/3} z^{-5/3}$		$\left(F_o = \dfrac{gQ}{\rho_o C_p T_o}\right)$
	A	B	$V/\sqrt{2g\Delta T z/T_o}$	$V/(Q\Delta T)^{1/5}\ \dfrac{m/s}{(kW\ K)^{1/5}}$	
Yokoi [4]	3.9	9.1	.90	.62	Alcohol Point Source
Yih [8]	4.7	11.0	1.0	.72	Bunsen Burner
George [9]	3.4	9.1	.80	.54	Heated Air Jet
(17)	3.6	9.5	.83	.57	Plume
Heskestad [3]				<.50>	Best Estimate into Flame Region for Q = 40-25000 kW
Present	3.7	8.0	.93	.61	Natural Gas with Radiation Loss
			$(A/\sqrt{2B}\ )$	$(.25\ A/B^{1/5})$	

28
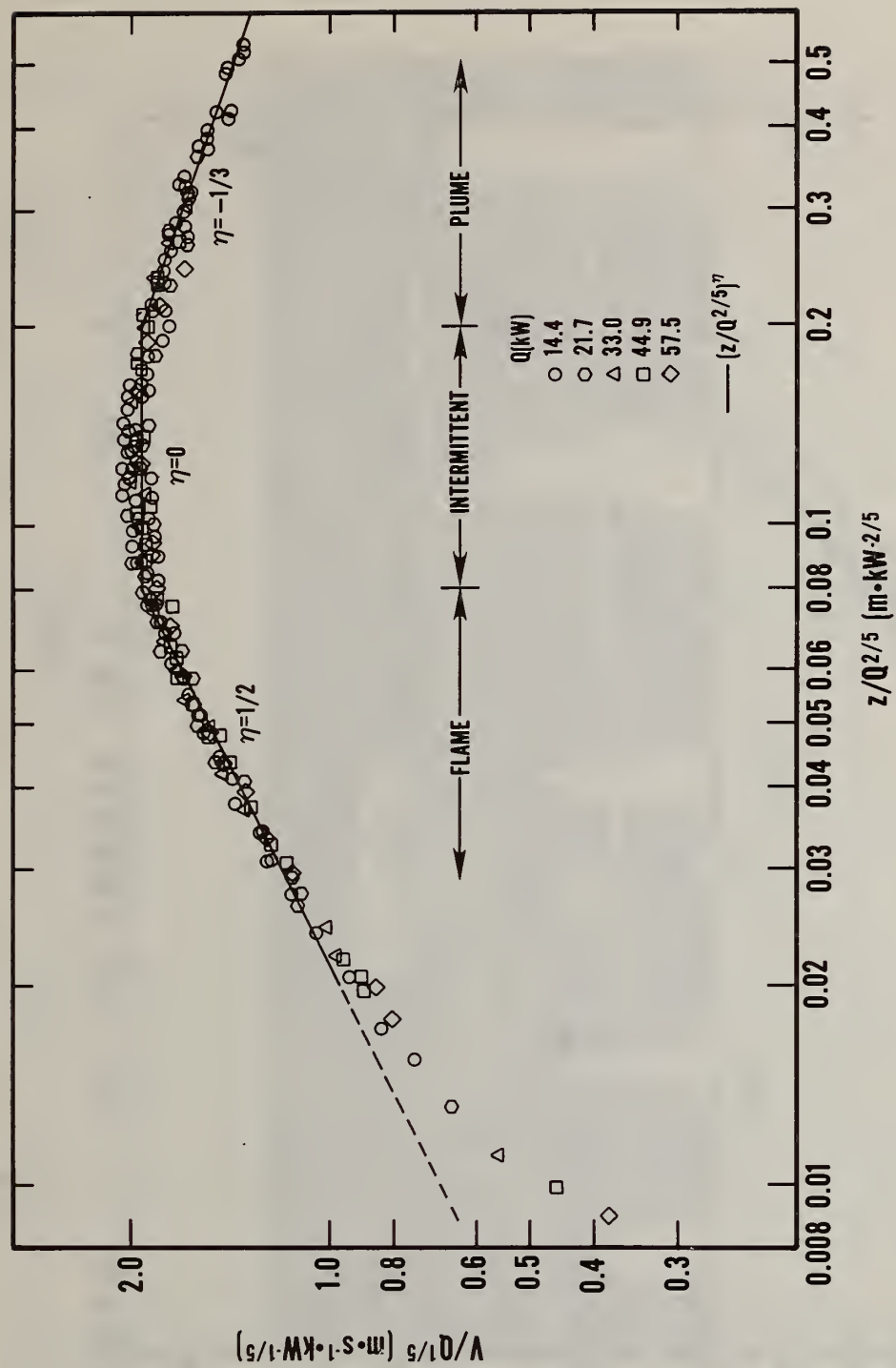
Figure 1. Center line velocity vs height

29
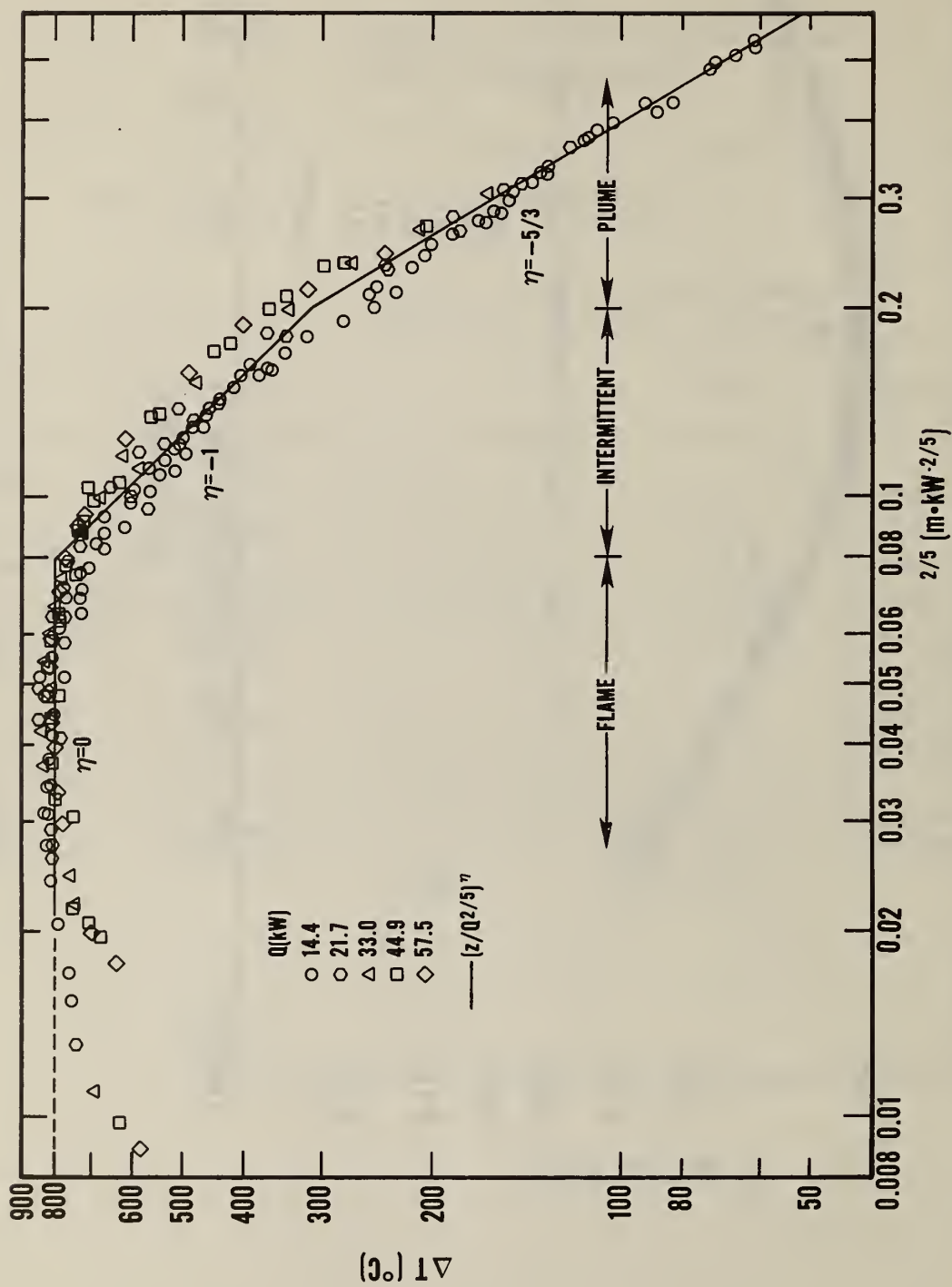
Figure 2. Center line temperature rise vs height
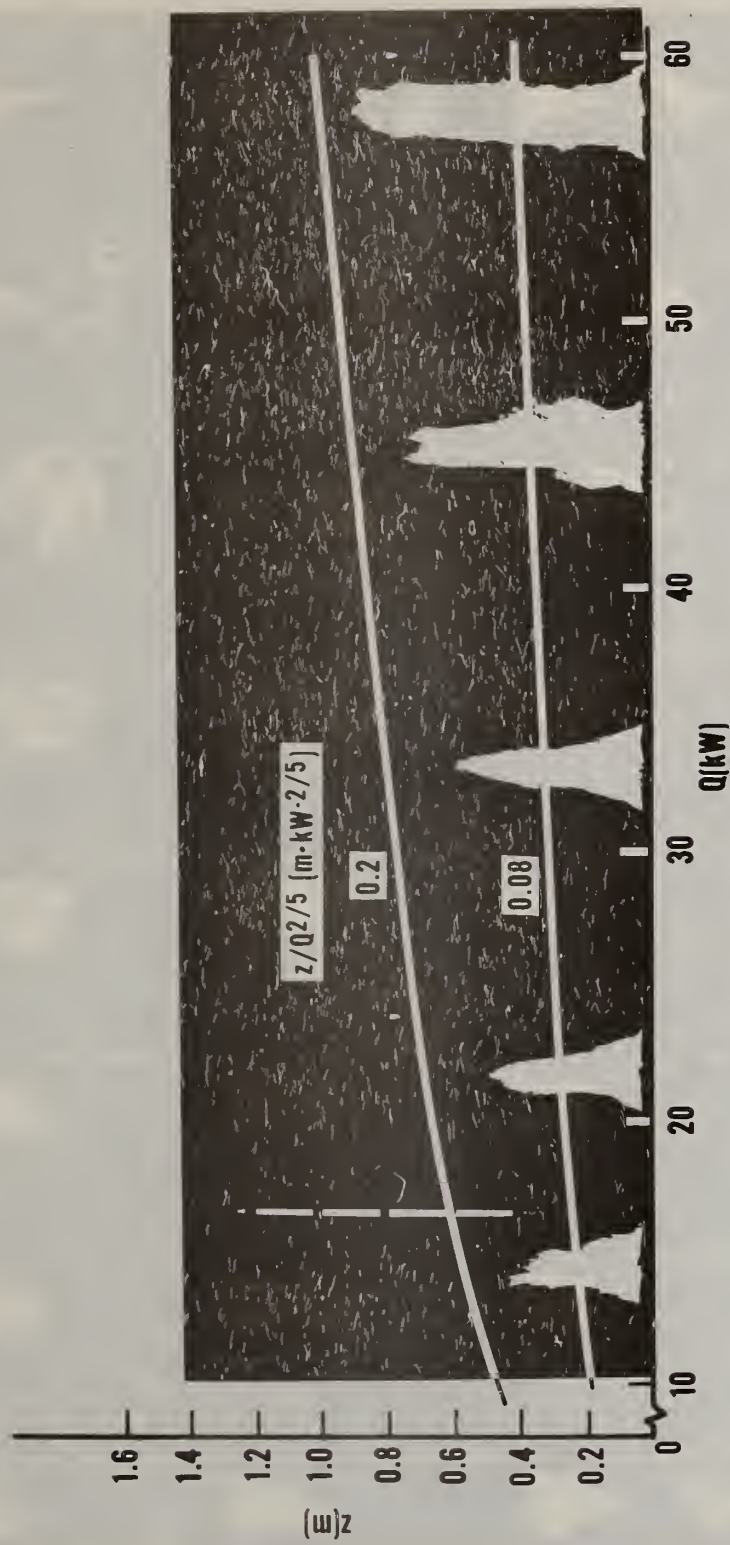
Figure 3. One-second time exposed flame photos vs heat release rate
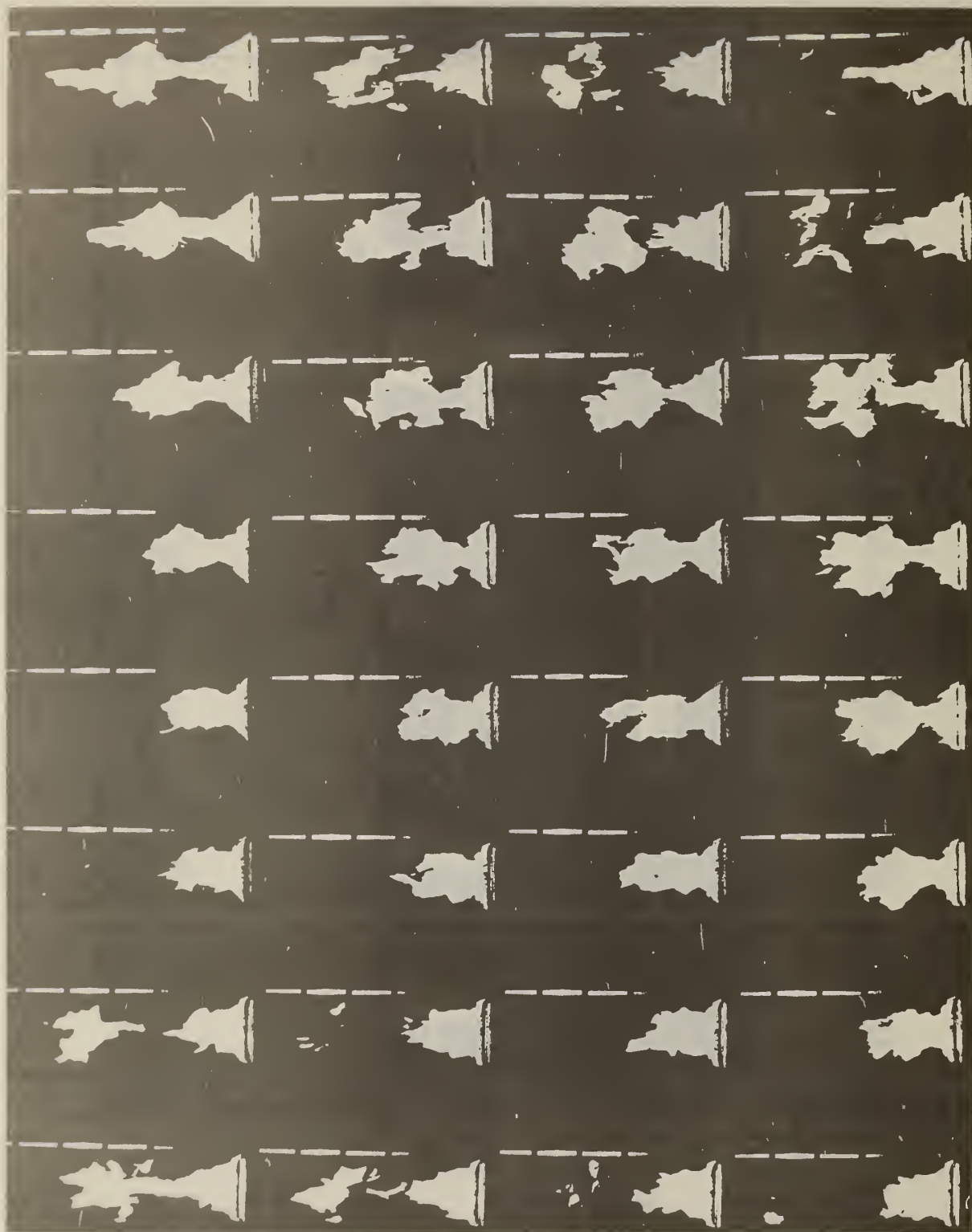
Figure 4. One and one-third seconds of cine film (24 frames/s) showing 3 Hz (eight frames) oscillation
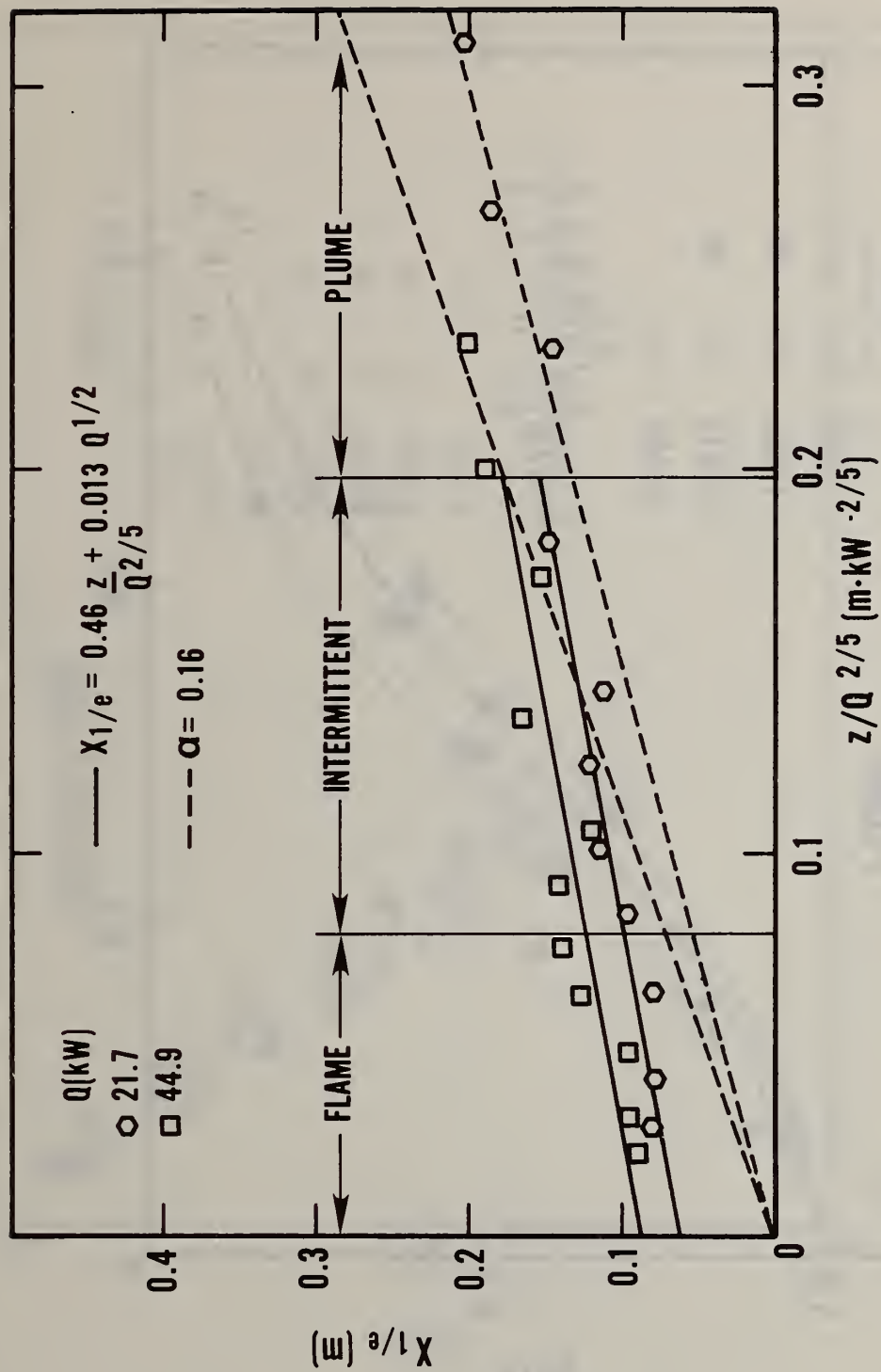
Figure 5. Width of velocity profile vs height
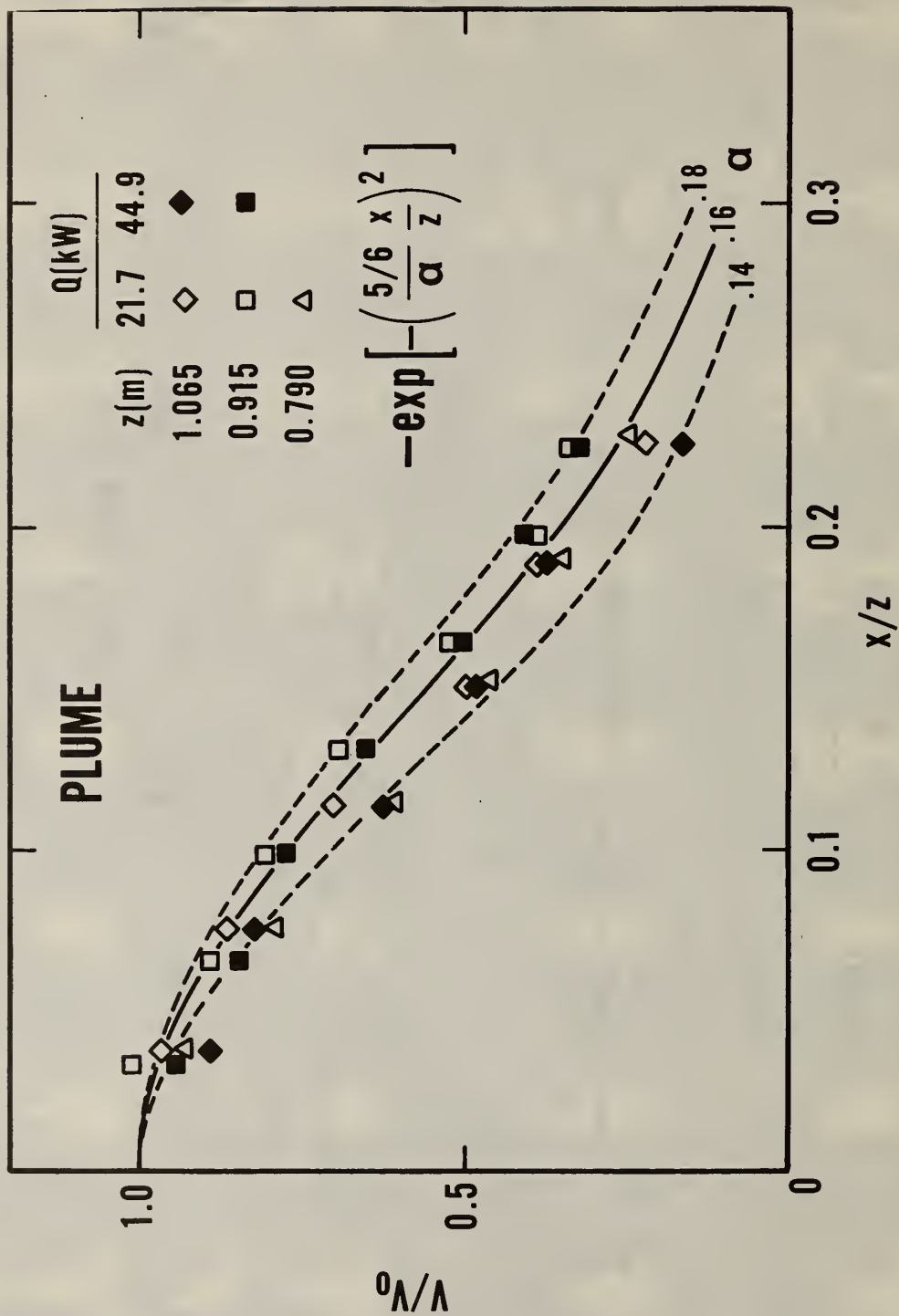
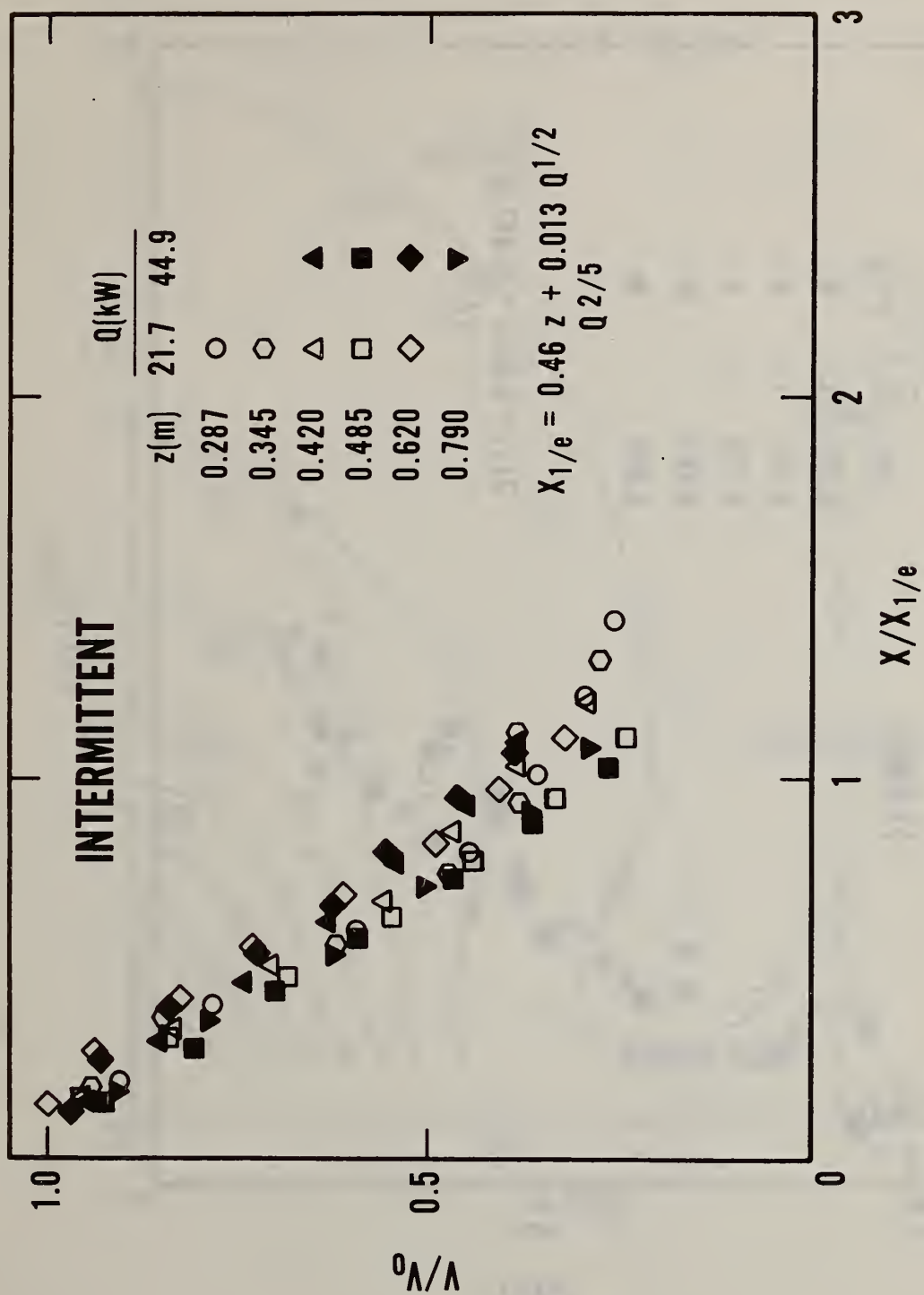Figure 6. Velocity profile in plume
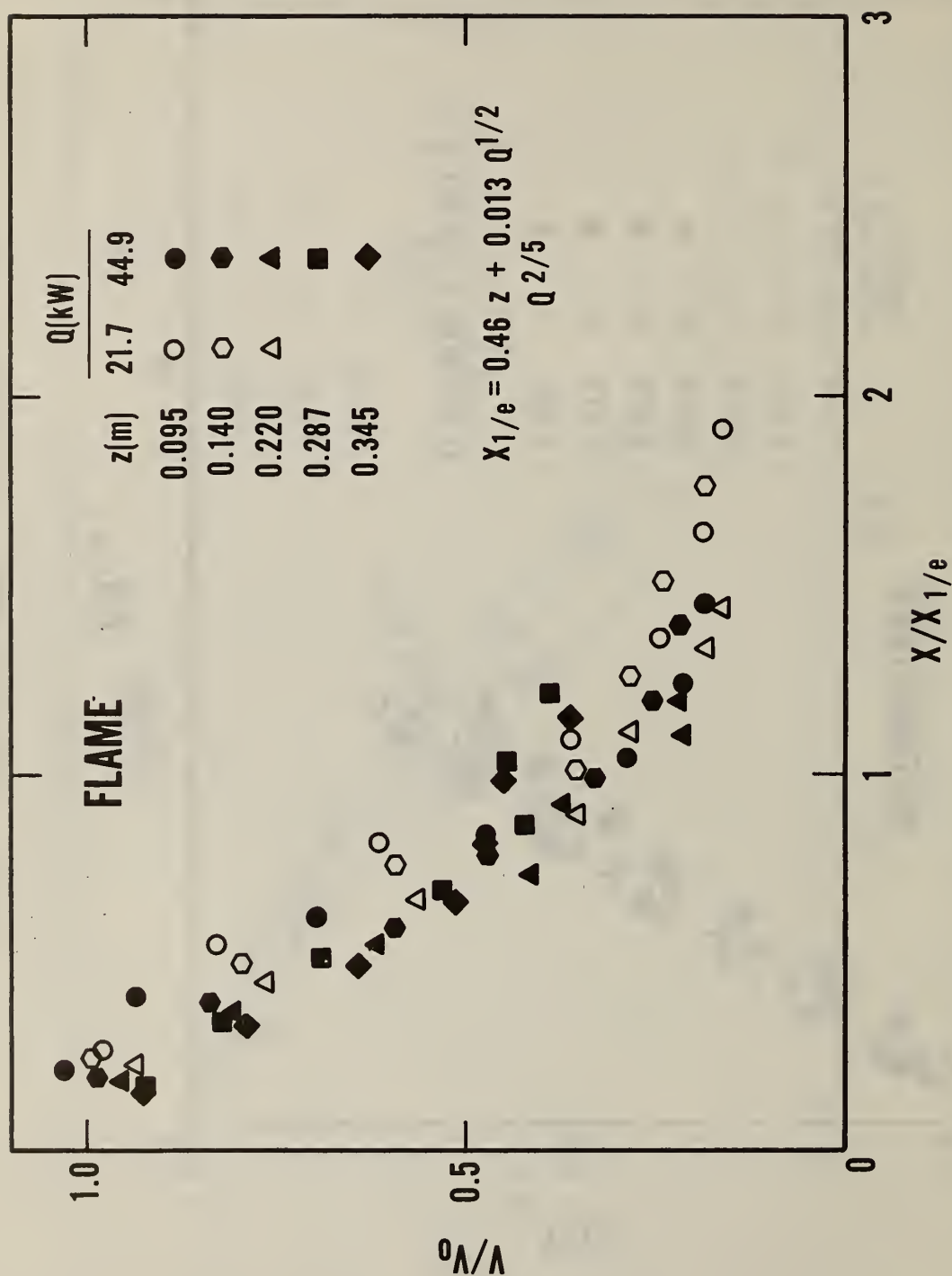
Figure 7. Velocity profile in intermittent region
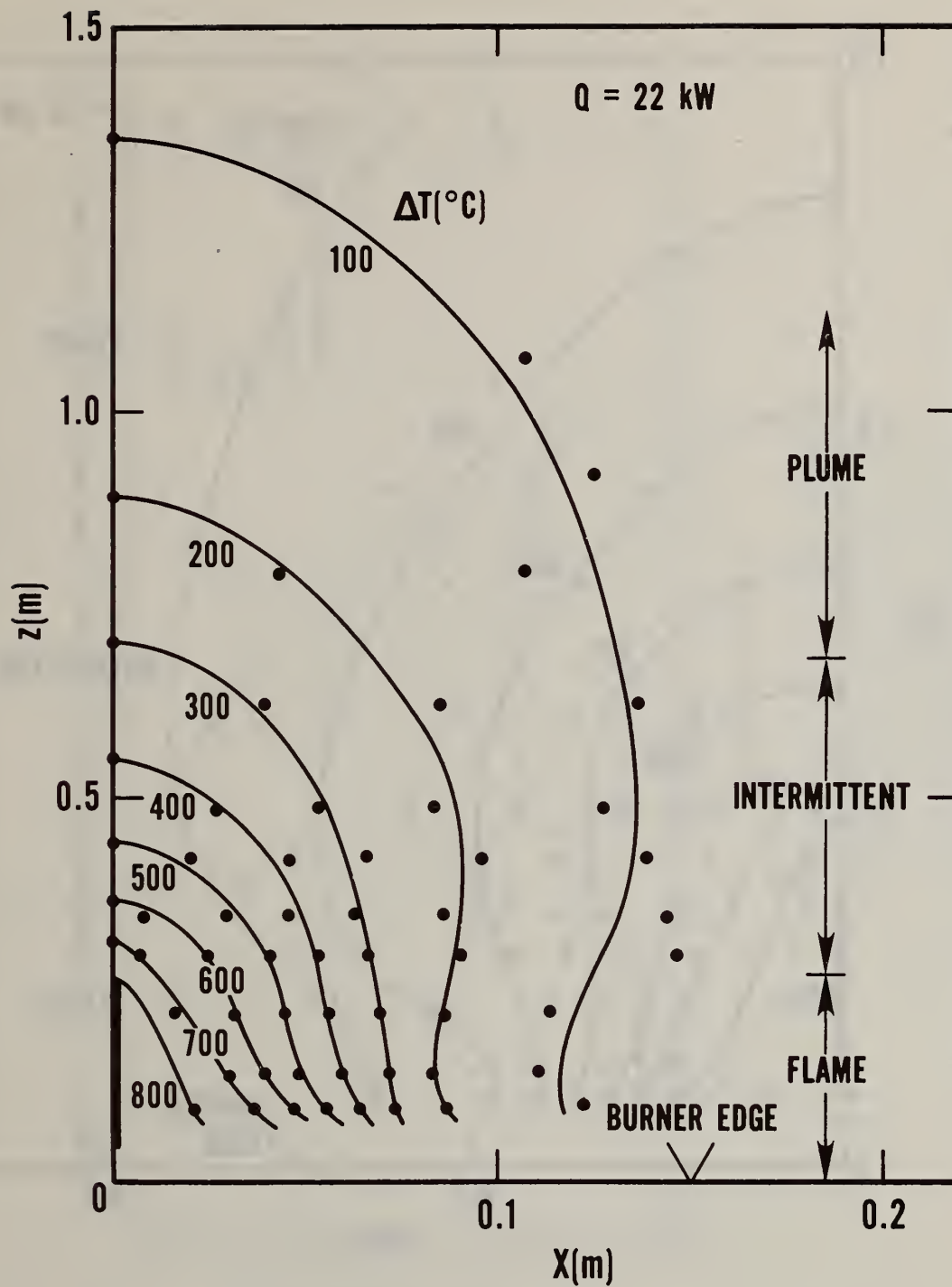
Figure 8. Velocity profile in flame region

$X_{1/e} = 0.46 z + 0.013 \dfrac{Q^{1/2}}{Q^{2/5}}$

FLAME

z(m)	$\overline{\text{21.7}}$	$\dfrac{Q(kW)}{44.9}$
0.095	○	●
0.140	◯	⬟
0.220	△	▲
0.287		■
0.345		◆

V/V₀

X/X₁/ₑ

Figure 9. Temperature rise in space coordinates, Q = 22 kW
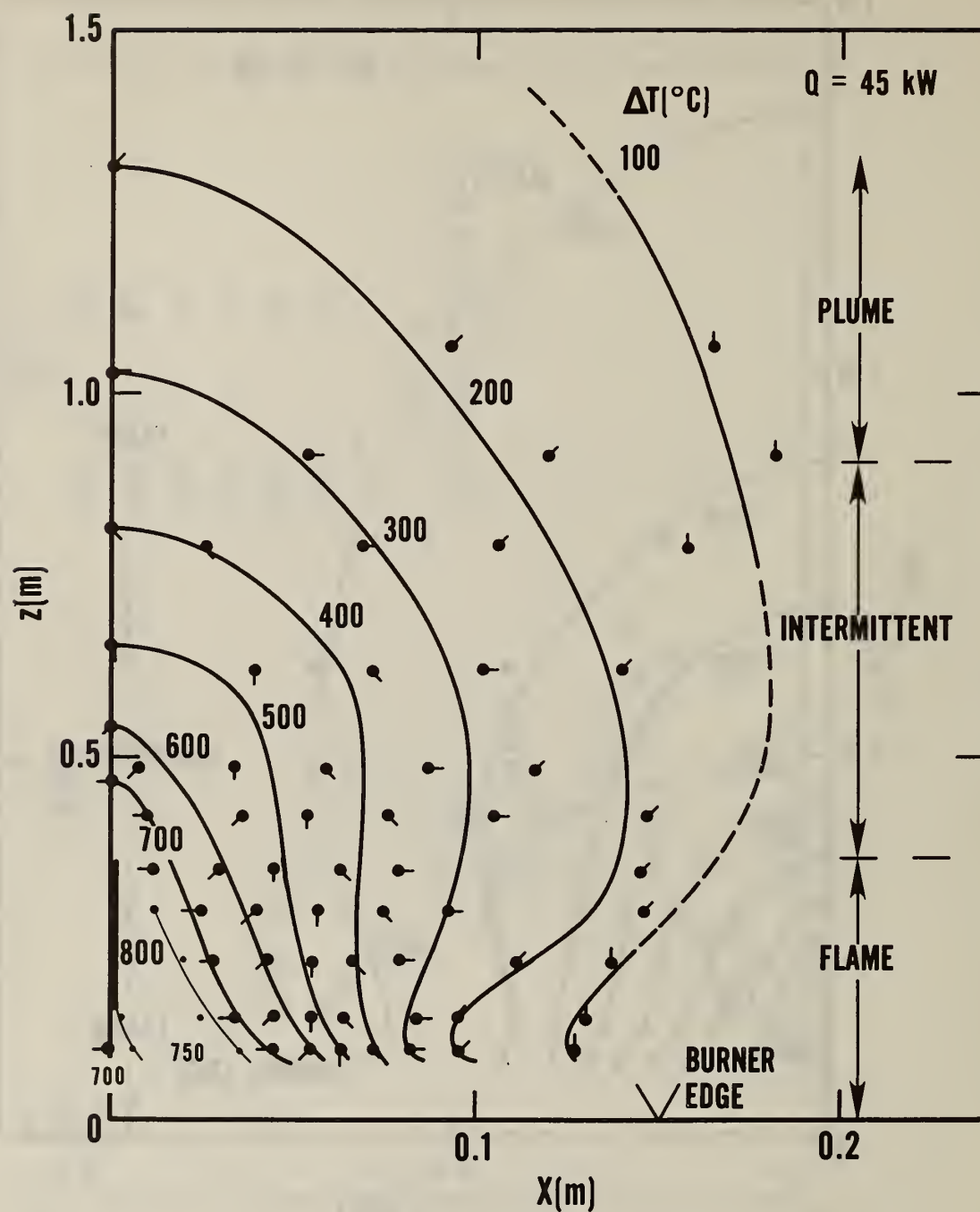
Figure 10. Temperature rise in space coordinates, Q = 45 kW
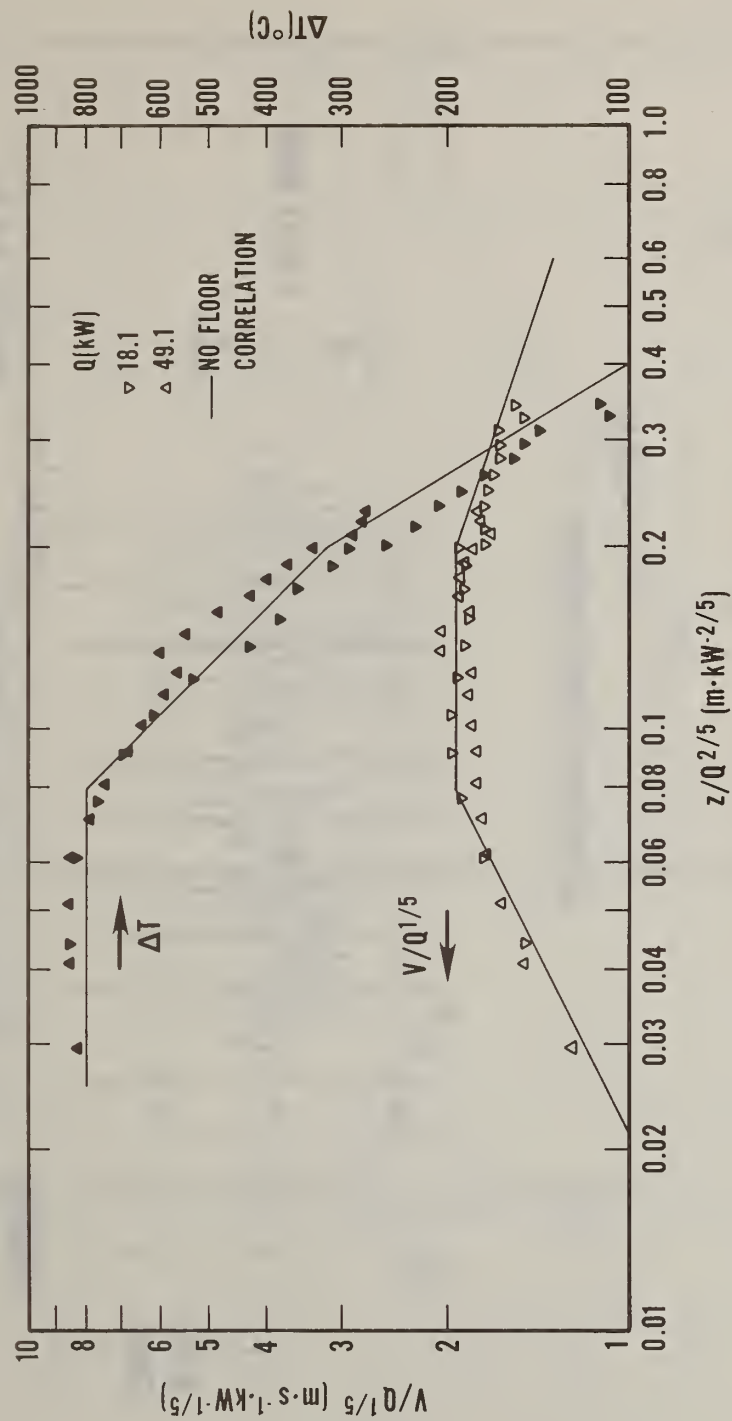
Figure 11. Velocity and temperature rise vs height
for simulated floor configuration
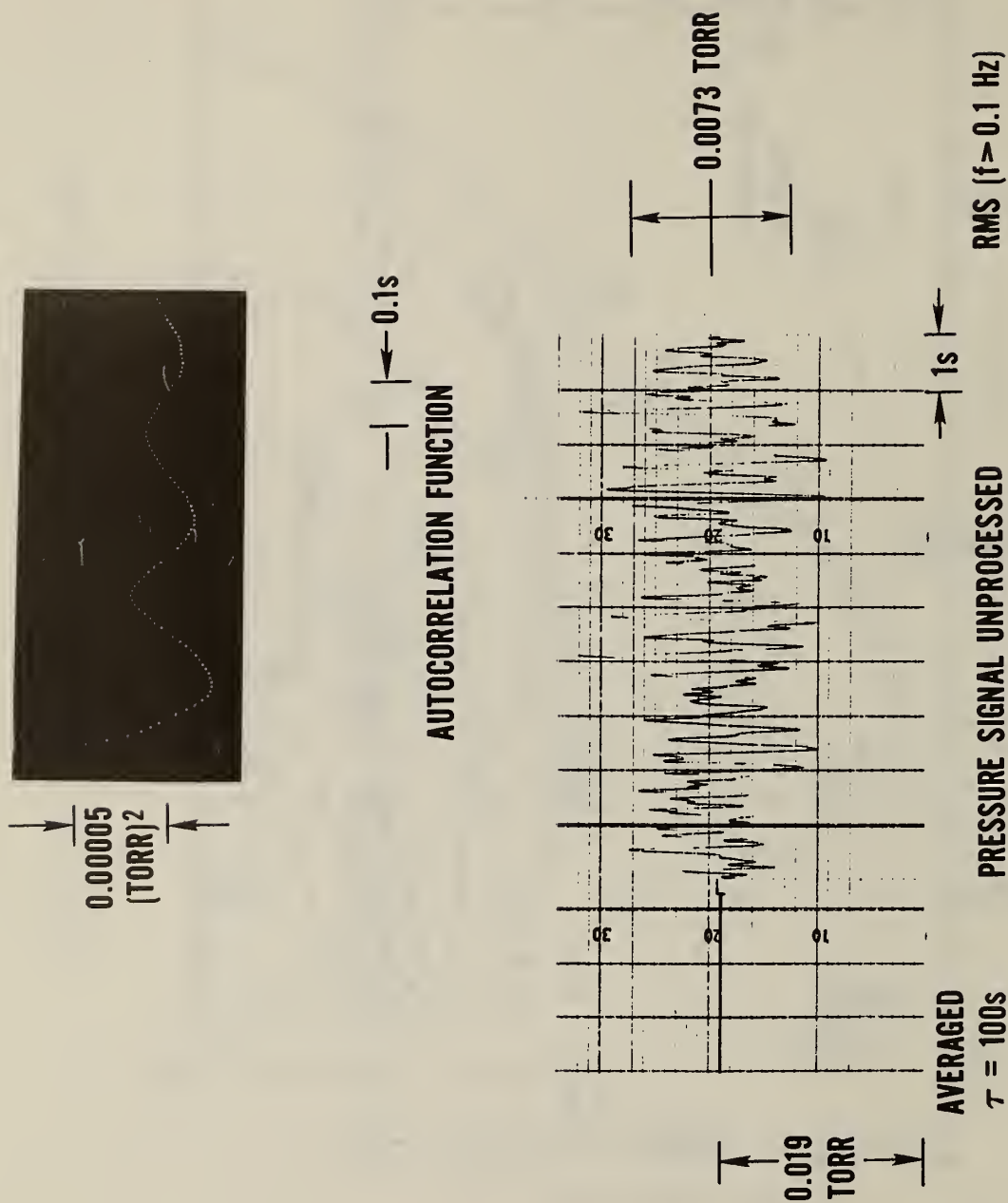
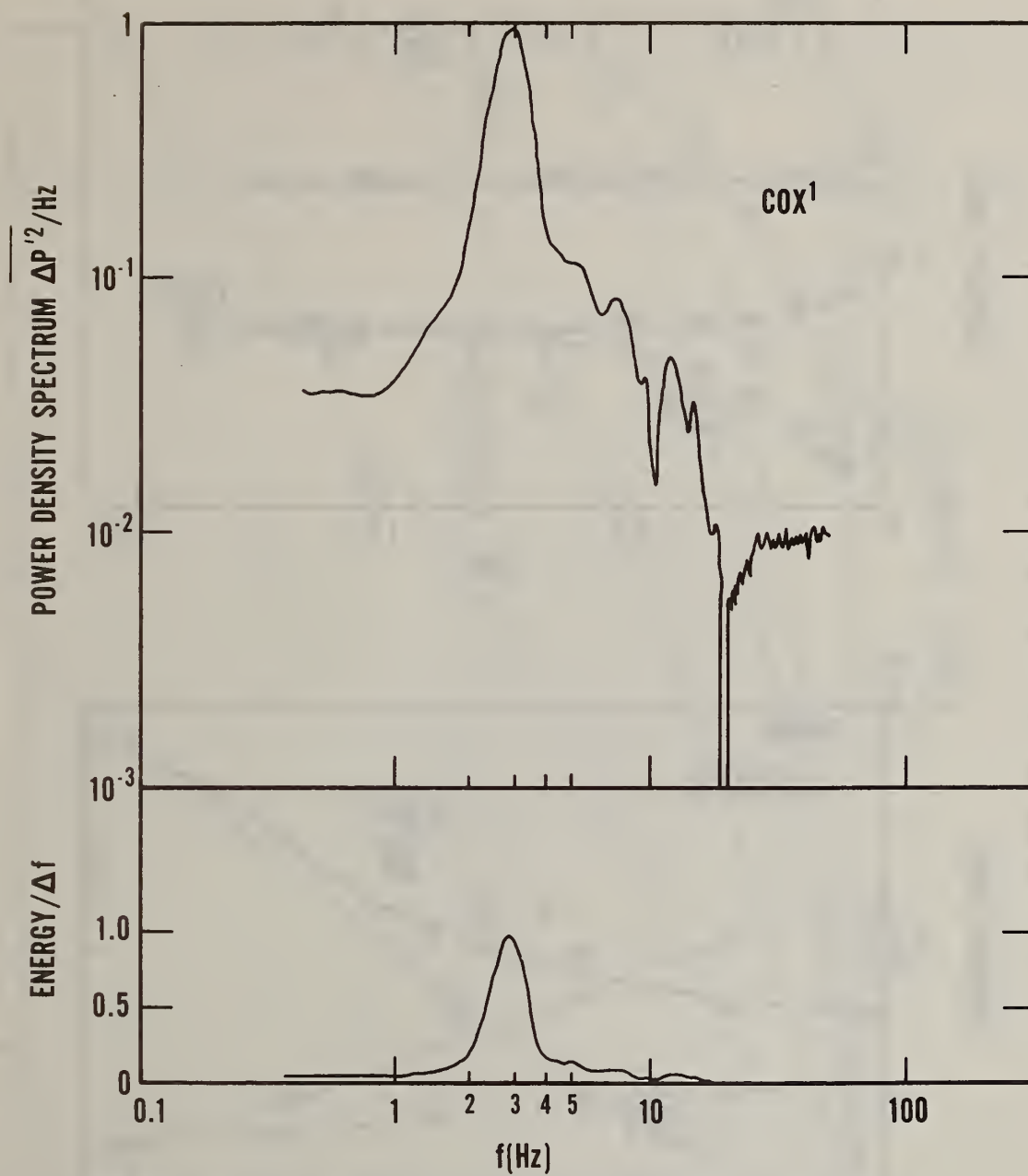Figure 12. Unprocessed, time-averaged, RMS, and auto-correlation signals of Δp output

Figure 13. Power density spectrum and energy distribution
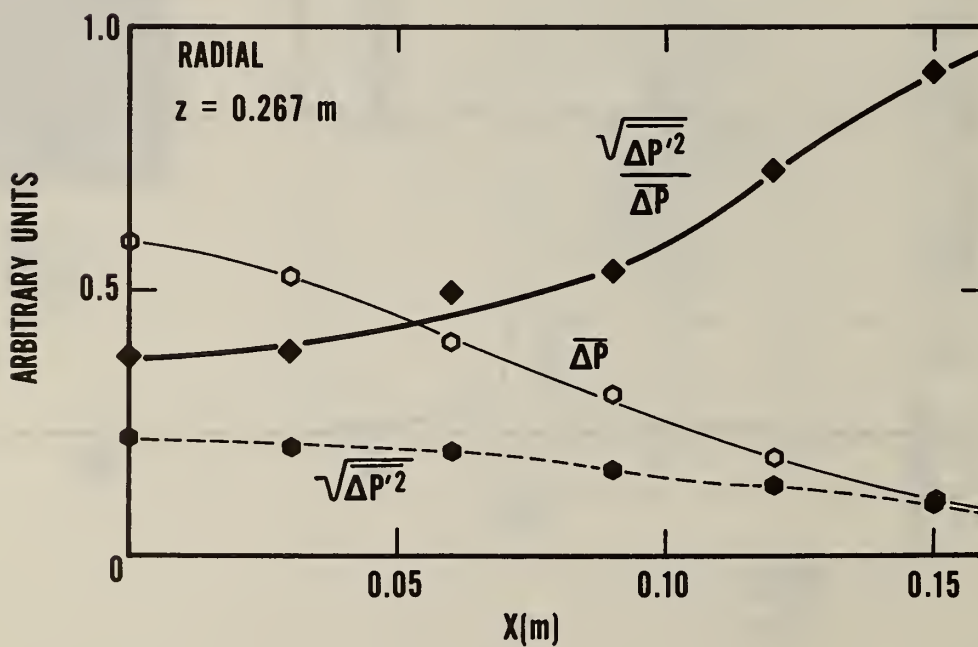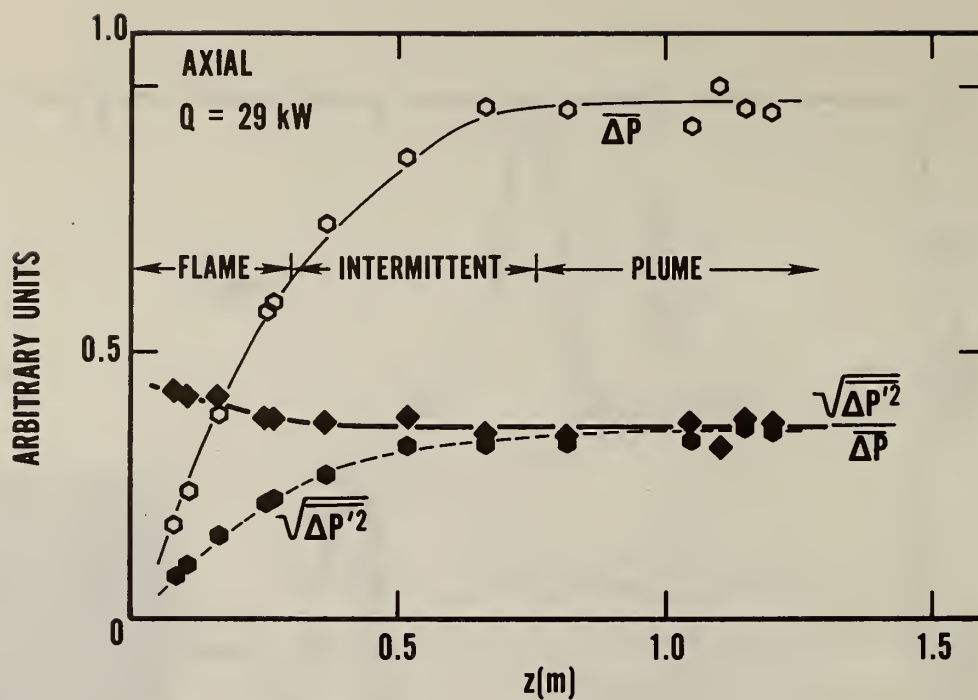of pressure signal vs frequency

41

Figure 14. Time-averaged and RMS component of
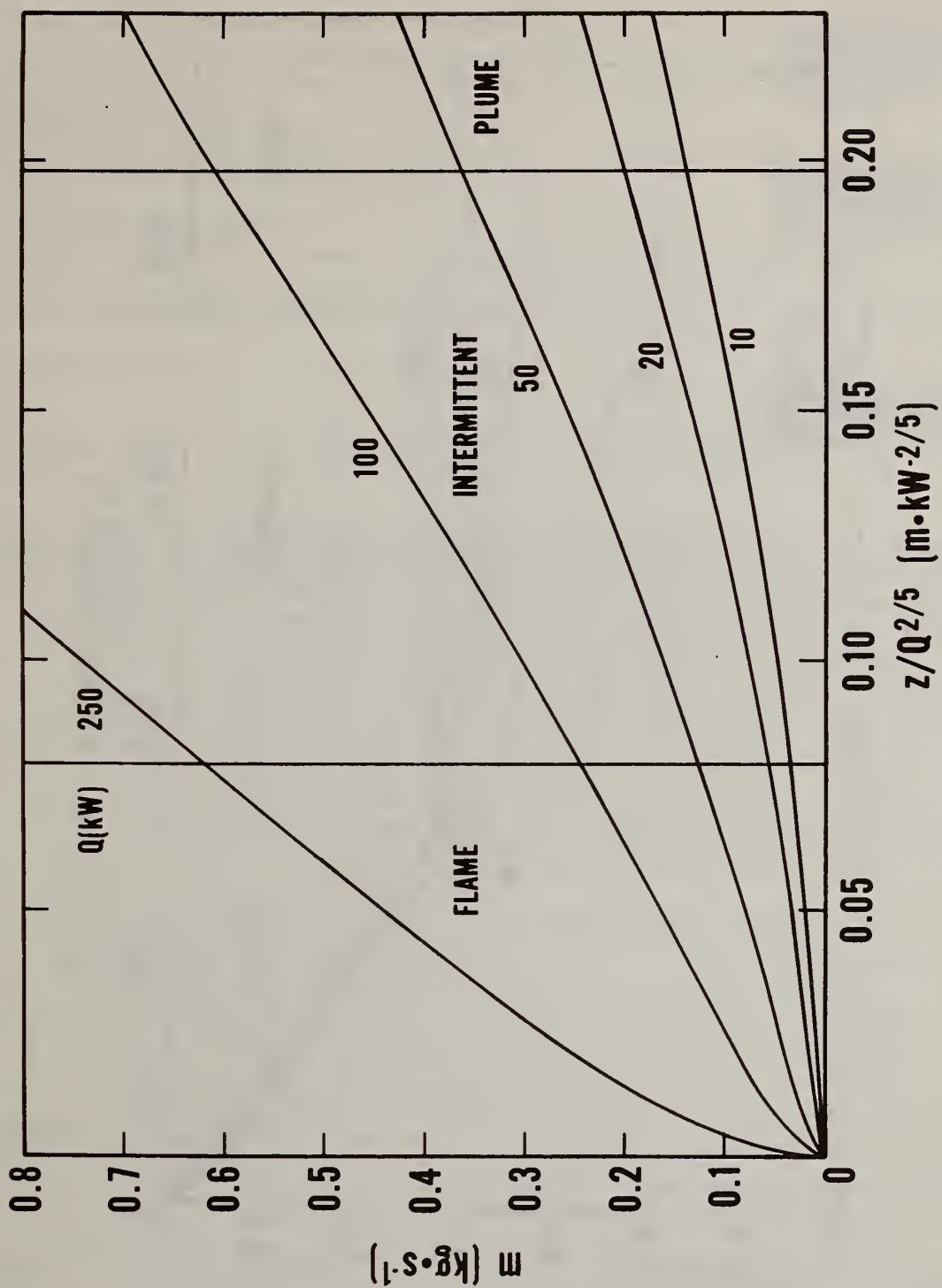pressure signal axially and radially

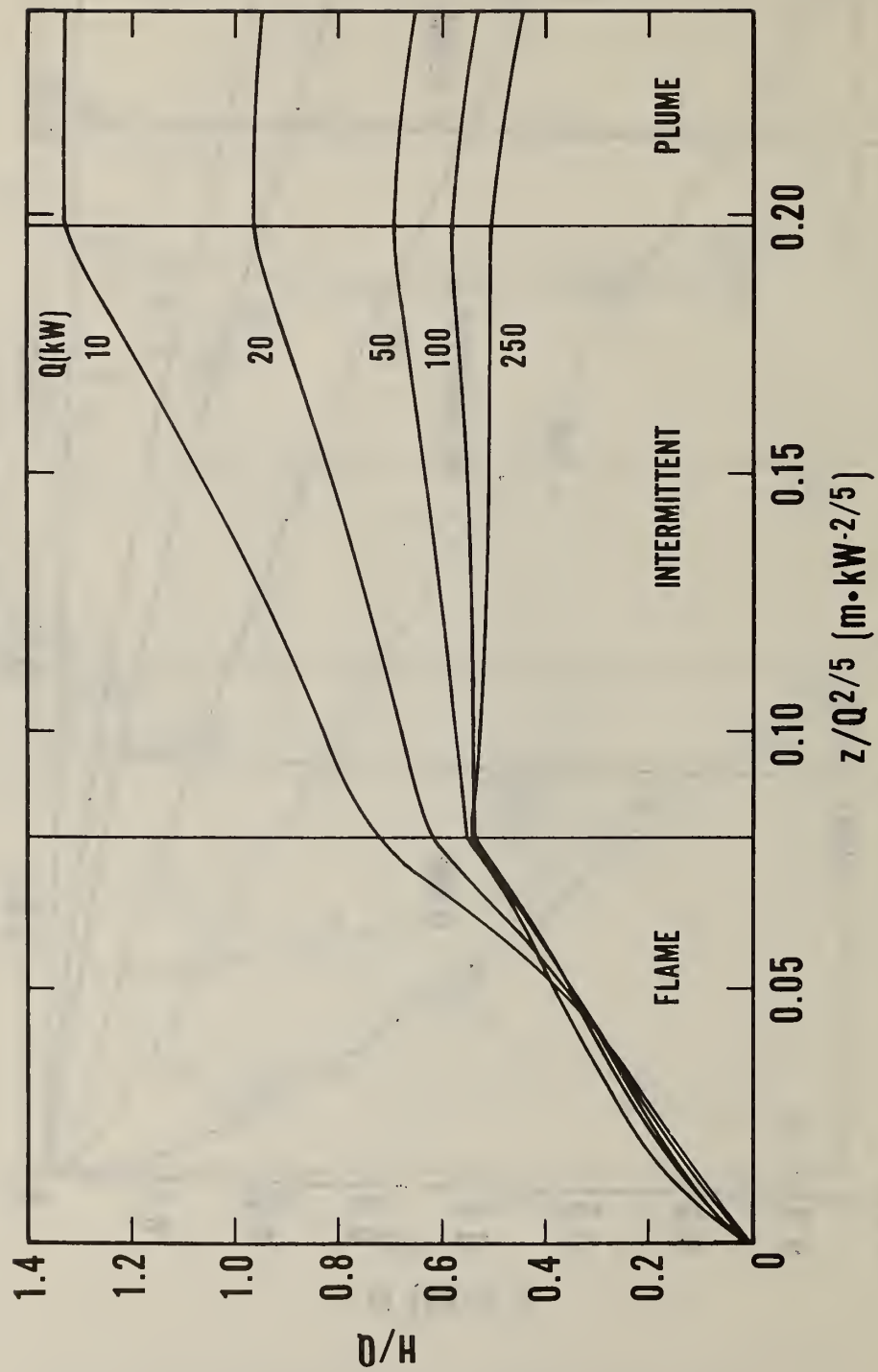Figure 15. Entrained mass flow vs height for various heat release rates

Figure 16. Normalized convective flux vs height for various heat release rates

U.S. DEPT. OF COMM. BIBLIOGRAPHIC DATA SHEET	1. PUBLICATION OR REPORT NO. NBSIR 79-1910	2. Gov't. Accession No.	3. Recipient's Accession No.

4. TITLE AND SUBTITLE

PURELY BUOYANT DIFFUSION FLAMES: SOME EXPERIMENTAL RESULTS

5. Publication Date

October 1979

6. Performing Organization Code

7. AUTHOR(S)

Bernard J. McCaffrey

8. Performing Organ. Report No.

9. PERFORMING ORGANIZATION NAME AND ADDRESS

NATIONAL BUREAU OF STANDARDS
DEPARTMENT OF COMMERCE
WASHINGTON, DC 20234

10. Project/Task/Work Unit No.

11. Contract/Grant No.

12. SPONSORING ORGANIZATION NAME AND COMPLETE ADDRESS *(Street, City, State, ZIP)*

(same as above)

13. Type of Report & Period Covered

Final

14. Sponsoring Agency Code

15. SUPPLEMENTARY NOTES

☐ Document describes a computer program; SF-185, FIPS Software Summary, is attached.

16. ABSTRACT *(A 200-word or less factual summary of most significant information. If document includes a significant bibliography or literature survey, mention it here.)*   Measurements of temperature and velocity using thermocouples and an impact probe were made in the near field of a purely buoyant diffusion flame produced by a porous refractory burner. Based on time-averaged center line value of V and ΔT together with photographic records the flame can be conveniently divided into three distinct regimes: (1) a continous flame region, starting from the surface of the burner with V equal to zero at the surface and rising with the height above the burner, z, to the 1/2 power. ΔT is constant over this regime. Higher up is (2), an intermittent regime, with pulsating flame (~3 Hz) exhibiting approximately constant V and ΔT falling with z to the first power. Still higher is (3) the plume region which is, most of the time, free of flames with $V \sim z^{-1/3}$ and $\Delta T \sim z^{-5/3}$ as predicted by conventional plume theory. Throughout the three regimes and indistinguishable among these is the consistency of the buoyancy relation, $V/\sqrt{2gz \, \Delta T/T_o}$ which has a value of approximately 0.9, a factor 2.5 times previous estimates in the flame region and confirming the recent correlation measurements of Cox[1]. Different heat release rates, Q, can be scaled to a "universal" fire if the length is normalized as $z/Q^{2/5}$ and the velocity scale as $V/Q^{1/5}$. The flame regime is thus independent of Q.

In the radial direction for time-averaged quantities only the plume region appears reasonably Gaussian. The data in the flame and intermittent regimes do not fall as rapidly as that dictated by a Gaussian distribution. In all three regimes the velocity profile is <u>wider</u> than the temperature profile.

Large scale, low frequency Δp fluctuations are about 35% of the time-averaged signal on the center line throughout the three regions. Radially the fluctuating to time-averaged signal ratio rises from the center line value and approaches 100% in the wings. Elementary spectral analysis indicates that most of this energy is concentrated in a narrow band centered around 3 Hz.

Implications of these results for flame entrainment calculations and heat release rates will be discussed.

17. KEY WORDS *(six to twelve entries; alphabetical order; capitalize only the first letter of the first key word unless a proper name; separated by semicolons)*

Buoyancy; diffusion flames; fire entrainment; flame oscillations; plume; scaling.

18. AVAILABILITY ☒ Unlimited	19. SECURITY CLASS (THIS REPORT) UNCLASSIFIED	21. NO. OF PRINTED PAGES 49
☐ For Official Distribution. Do Not Release to NTIS		
☐ Order From Sup. of Doc., U.S. Government Printing Office, Washington, DC 20402, SD Stock No. SN003-003-	20. SECURITY CLASS (THIS PAGE)	22. Price
☒ Order From National Technical Information Service (NTIS), Springfield, VA. 22161	UNCLASSIFIED	$4.50